often referred to as facultative stem/progenitor cells in the adult liver (Alison et al. 1996; Yanger and Stanger 2011).

There are several experimental models to induce LPCs. In mice, 3,5-diethoxycarbonyl-1,4-dihydrocollidine (DDC) diet and choline-deficient, ethionine-supplemented (CDE) diet models are often used (Preisegger et al. 1999; Akhurst et al. 2001). The LPC response, also termed as ductular reaction, has been found in human chronic liver diseases and severely injured livers, such as acute hepatitis, fulminant hepatitis, cholestatic disorders, and liver cancers (Libbrecht and Roskams 2002; Turanyi et al. 2010). This suggests that LPCs are broadly activated to restore the function of the liver when mature hepatocytes fail to proliferate. Despite previous notions that the degree of the LPC response correlates with the severity of liver disease (Lowes et al. 1999), it has not been demonstrated whether LPCs indeed engage in liver regeneration. In addition, the underlying mechanism of the activation of LPCs still remains largely unknown.

As liver injuries accompanying the LPC responses are usually associated with inflammation and fibrosis, interaction between LPCs and multiple other cell populations, such as immune cells and fibroblastic cells, has been postulated. In many cases of adult stem/progenitor cell regulation, the importance of the extracellular signals provided by the surrounding cells, forming the so-called stem cell niche, are well recognized. However, little has been documented as to whether and how the LPCs are regulated by the niche signals. Cell-to-cell interactions involve paracrine growth factors and cytokines that can be grouped into several major families (Gerhart 1999), among which the fibroblast growth factor (FGF) family is one of the best characterized. FGFs constitute a family of growth factors that have diverse activities in development and adulthood. It has been reported that FGF signals participate in tissue development and organization, branching morphogenesis, angiogenesis, and wound repair, as well as the regulation of stem cell systems in various organs (Itoh and Ornitz 2008; Turner and Grose 2010). The mammalian FGF family is classified as paracrine (canonical) ligands, endocrine ligands, and FGF homologous factors. The paracrine FGF families can be further subdivided into five subfamilies—FGF1/2, FGF3/7/10/22, FGF4/5/6, FGF8/17/18, and FGF9/16/20—in mice and humans. There are four members of the FGF receptor family: FGFR1, FGFR2, FGFR3, and FGFR4. Since FGFR1, FGFR2, and FGFR3 each have splice variant isoforms "b" and "c," seven different FGFR subtypes can be expressed. It is known that their specific functions are achieved by spatially and temporally regulated expression patterns of particular ligands and receptors; for example, the FGF3/7/10/22 subfamily ligands are typically expressed by mesenchymal cells and exert their effects through the cognate receptor FGF receptor 2 isoform IIIb (FGFR2b), whose expression is restricted in epithelial cells (Steiling and Werner 2003).

In the present study, we aimed at elucidating the cellular and molecular framework that underlies the LPC regulation upon liver injury. Based on the characteristic expression profile and the results of in vivo functional analyses, we found evidence that FGF7 is an essential signal for induction of the LPC response and contributes to the progenitor-dependent liver regeneration.

Results

Thy1$^+$ cell population is a candidate for the LPC niche

As previous studies have suggested that nonepithelial populations such as mesenchymal cells and immune cells reside near and around LPCs (Paku et al. 2001; Knight et al. 2007; Strick-Marchand et al. 2008), we suspected that those cells may functionally interact with LPCs and provide a putative LPC niche. To identify and characterize such an LPC–niche interaction, we first induced the LPC response in the mouse liver with a well-established protocol of the hepatotoxin DDC diet application (Preisegger et al. 1999). Cytokeratin 19$^+$ (CK19$^+$) LPCs expanded from around the portal vein after liver damage by feeding DDC diet (Fig. 1A). Immunostaining of the liver sections with several cell surface markers led to the finding that a Thy1$^+$ cell population appeared in close proximity to LPCs in DDC-induced liver damage (Fig. 1A). We selected and focused on this marker for further analysis, as its expression in injured livers has also been described in rats and humans (Dezso et al. 2007; Yovchev et al. 2009). An established marker for fibroblastic cells (Elastin) and a stellate cell marker (Desmin) partially overlapped with the Thy1$^+$ area (Supplemental Fig. S1A,B). Quantitative analysis of the Thy1 and CK19 immunostaining revealed that the expansion of Thy1$^+$ cells occurred prior to LPC activation (Fig. 1B). Thus, we presumed that Thy1$^+$ cells could provide a niche for LPCs that allows them to proliferate.

We sought to identify the nature of the niche signals for LPCs possibly provided by Thy1$^+$ cells. Among several major groups of paracrine factors, we especially focused on the FGF family because an LPC-specific marker, Trop2 (Okabe et al. 2009), has previously been reported as a target gene of FGF10 in lung development (Lu et al. 2005). We analyzed expression patterns of all of the paracrine *Fgf* ligands and found *Fgf7* to be highly expressed, while we could not detect any expression of *Fgf10* or *Fgf3/22* belonging to the same subfamily (Supplemental Fig. S2). The expression of *Fgf7* was increased significantly during the time course of DDC-induced liver damage, along with that of *Epcam* and *Krt19*, encoding the LPC/BEC markers epithelial cell adhesion molecule (EpCAM) and CK19, respectively (Fig. 1C). Accordingly, expression of FGF7 protein was barely detected in normal livers but was markedly induced in the vicinity of LPCs after DDC (Fig. 1D,F). Intriguingly, some Thy1$^+$ cells costained with FGF7 in the injured liver (Fig. 1E). We also examined a recovery model for liver injury, where mice were initially fed a DDC diet for 4 wk and then returned to the normal diet for another 2 wk (Supplemental Fig. S3). In this injury/recovery setting, the overall level of *Fgf7* expression strongly correlated with that of the LPC response as well as the progression of liver damage as measured by serum markers. These results suggest that FGF7 is a strong candidate for the niche signal for LPCs.

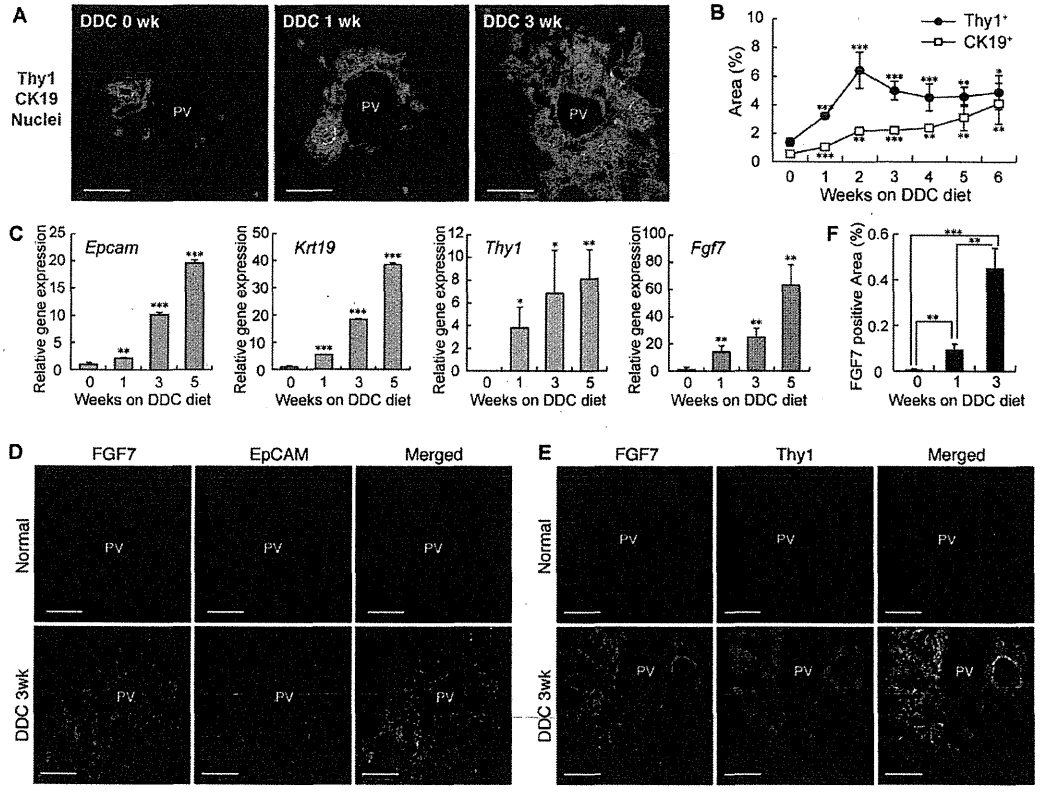

Figure 1. FGF7 expression in the damaged liver is up-regulated around LPCs. (*A*) Liver sections prepared from DDC diet-fed mice were subjected to immunofluorescent double-staining analysis. Thy1$^+$ cells (green) were observed in the immediate vicinity of CK19$^+$ LPCs (red) during the course of LPC activation. Bars, 80 μm. (PV) Portal vein. (*B*) Thy1- and CK19-positive areas were increased in the DDC-treated livers, as determined by quantitative analysis of immunofluorescence-stained images. Mean ± SD ($n = 3$). (***) $P < 0.001$; (**) $P < 0.01$; (*) $P < 0.05$, compared with normal liver (0 wk). (*C*) Total RNA was isolated from whole-liver samples of normal diet-fed (0 wk) or DDC diet-fed mice, reverse-transcribed, and subjected to quantitative PCR analyses to determine expression of the LPC markers *Epcam* and *Krt19*, the mesenchymal cell marker *Thy1*, and *Fgf7*. Expression was normalized to that of *Gapdh*. Mean ± SD ($n = 3$). (***) $P < 0.001$; (**) $P < 0.01$; (*) $P < 0.05$, compared with the value at 0 wk. (*D*,*E*) Confocal immunofluorescence images of the livers show that FGF7 (green) protein localized in the proximity of EpCAM$^+$ LPCs (*D*, red) and colocalized with Thy1$^+$ mesenchymal cells (*E*, red) in the periportal region in injured livers. Bars, 50 μm. (PV) Portal vein. (*F*) Expression of FGF7 protein was increased in the DDC-treated livers, as determined by quantitative analysis of immunofluorescence-stained images of at least 11 periportal fields from three livers for each time point. Mean ± SE. (***) $P < 0.001$; (**) $P < 0.01$.

LPCs receive the FGF7 signal from Thy1$^+$ mesenchymal cells

To determine whether FGF7 can act on LPCs directly, we analyzed the expression of the FGF7 receptor FGFR2b in LPCs. In situ hybridization analysis of liver sections detected expression of the *Fgfr2* transcript in the CK19$^+$ LPC population (Fig. 2A). To validate expression of the cognate isoform for FGF7, EpCAM$^+$ LPCs and EpCAM$^-$ cells were isolated from the nonparenchymal cell (NPC) population of the DDC-treated liver and immunostained with a IIIb isoform-specific anti-FGFR2 antibody. We detected strong expression of FGFR2b in EpCAM$^+$ cells but not in EpCAM$^-$ cells (Fig. 2B,C).

We next performed quantitative PCR analysis using specific cell populations to further confirm the FGF7-producing cells and their target cells. Hepatocyte, NPC, EpCAM$^+$ LPC, Thy1$^+$ CD45$^-$ cell (Thy1$^+$ MC [for mesenchymal cell]) (see below), Thy1$^+$ CD45$^+$ cell (T-cell), and Thy1$^-$ CD45$^+$ cell (blood cell) fractions were isolated from the livers of mice fed DDC. We checked for adequate cell separation by the specific expression of each marker (Supplemental Fig. S3A). As expected from the aforementioned immunostaining patterns, *Fgf7* and *Fgfr2* isoform IIIb were detected in Thy1$^+$ MC and LPC fractions, respectively (Fig. 2D). These results suggest that FGF7 signal may function directionally from Thy1$^+$ CD45$^-$ cells to LPCs. The Thy1$^+$ CD45$^-$ cells strongly expressed *Elastin* (*Eln*), *nerve growth factor receptor* (*Ngfr*; p75NTR) and *α smooth muscle actin* (*Acta2*; α-SMA), which are markers for fibroblastic cells, hepatic stellate cells, and myofibroblasts, respectively (Fig. 2D; Supplemental Fig. S4A). Thus, they are considered to be a mesenchymal cell population and distinct from T-cell populations. We also

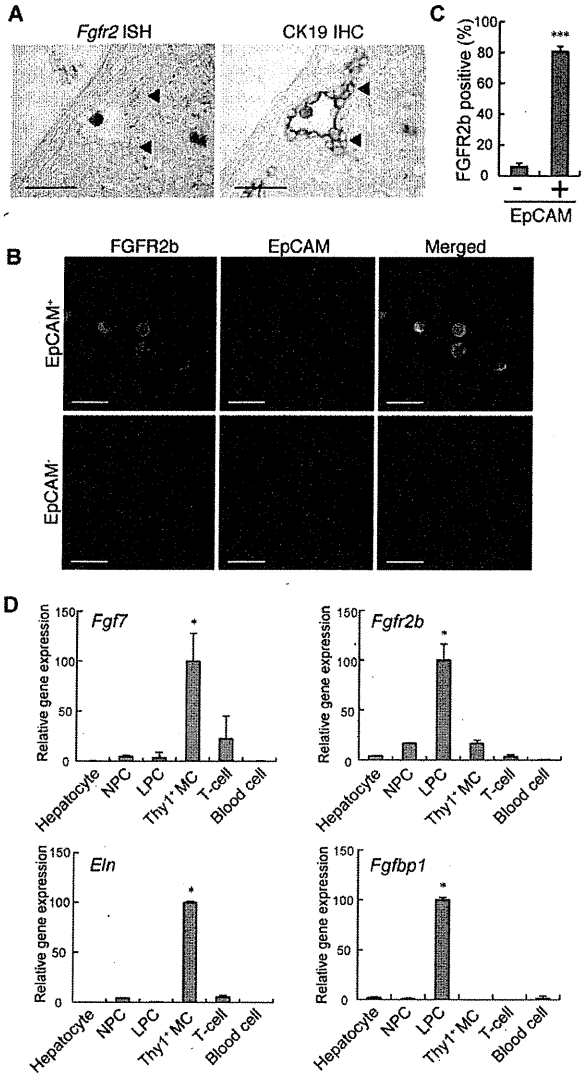

Figure 2. FGF7 signal emanates from Thy1$^+$ cells and acts on LPCs. (*A, left* panel) Liver sections prepared from mice fed DDC diet for 3 wk were subjected to in situ hybridization analysis for *Fgfr2* expression. (*Right* panel) The same section was subsequently overlaid with immunohistochemical staining using anti-CK19 antibody to confirm its expression in LPCs. Bars, 200 μm. (*B,C*) EpCAM$^+$ and EpCAM$^-$ cells were sorted from NPCs in the livers of the mice fed the DDC-containing diet for 5 wk. Cytospin preparations of these cells were stained for FGFR2b (green) and EpCAM (red). Representative images are shown in *B*, and the result of quantitation are shown in *C* (EpCAM$^-$, n = 980; EpCAM$^+$, n = 1454). Mean ± SD. Bars, 40 μm. (***) $P < 0.001$. (*D*) Hepatocyte, NPC, EpCAM$^+$ cell (LPC), Thy1$^+$ CD45$^-$ mesenchymal cell (Thy1$^+$MC), Thy1$^+$ CD45$^+$ T-cell (T-cell), and Thy1$^-$ CD45$^+$ cell (blood cell, excluding T-cell) fractions were isolated from the livers of DDC-treated mice. Expression of the indicated genes was examined by quantitative RT–PCR. Mean ± SD (n = 3). (*) Significantly different from each of the other five fractions (ANOVA, with Tukey post hoc tests, $P < 0.05$).

performed genetic lineage tracing experiments using an *Alfp-Cre* transgenic (Tg) mouse strain, where expression of the Cre recombinase occurred in fetal hepatoblasts and adult hepatocytes and hence enabled us to label and track their descendants. After DDC injury, hepatocytes, BECs, and LPCs were virtually all lineage-labeled. Thy1$^+$ cells, on the other hand, were of a distinct lineage from liver epithelial cells (Supplemental Fig. S4B,C).

FGF-binding protein 1 (FGFBP1) is a soluble protein that can bind a subset of FGFs, including FGF7, and enhance their activities (Beer et al. 2005). Previous studies on skin and renal tube regeneration have shown FGFBP1 to be expressed in epithelial cells rather than mesenchymal cells and to be a target of FGF7 signaling (Liu et al. 2001; Beer et al. 2005). *Fgfbp1* was almost exclusively expressed in LPCs, which further strengthened the notion that LPCs are the primary target of FGF7 signaling from Thy1$^+$ cells (Fig. 2D).

Up-regulation of FGF7 is concurrent with expansion of LPCs and Thy1$^+$ cells

We then examined the correlation of FGF7 with the induction of LPCs and Thy1$^+$ cells in other models of liver injury. First, ligation of the common bile duct (BDL) in mice was used as a model for cholestatic liver disease. FGF7 expression was increased in the BDL-manipulated liver with the LPC response (Fig. 3A,B). As is the case with DDC-induced liver injury, FGF7 in this model was also produced predominantly in Thy1$^+$ cells, while LPCs were the primary target for the signal by expressing the receptor (Supplemental Fig. S5). Second, we checked the activation of LPCs and expression of FGF7 in liver-specific *Tak1*-deficient (*Alfp-Cre*; *Tak1$^{flox/flox}$*, hereafter referred to as *Tak1*-LKO) mice. Loss of *Tak1* in the liver results in chronic inflammation and eventually leads to fibrosis and carcinogenesis (Bettermann et al. 2010; Inokuchi et al. 2010). It is thus considered a faithful model for the progression of human liver diseases. We observed apparent LPC response and expansion of Thy1$^+$ cells in 8-wk-old *Tak1*-LKO mice (Fig. 3C). Concomitantly with the increase of CK19-positive (Fig. 3E) and Thy1-positive (Fig. 3F) areas, the expression of FGF7 was significantly induced (Fig. 3D,G). Although the immunostaining results showed some colocalization of FGF7 with EpCAM$^+$ LPCs, gene expression analysis using isolated cell fractions confirmed that, also in this model, *Fgf7* was mainly produced in Thy1$^+$ cells but not in LPCs (Supplemental Fig. S6). Finally, serum FGF7 levels were found to be increased in human patients with liver diseases such as fulminant hepatic failure and acute hepatitis (Fig. 3H), which often accompany LPC activation. Together, these data suggest that induction of FGF7 upon liver disorders associated with the LPC response is generally conserved in both rodents and humans.

FGF7 plays a necessary function as a niche signal for induction of LPCs

To address the physiological relevance of FGF7 expression in the course of the LPC response, we used *Fgf7*

knockout mice (Guo et al. 1996). They exhibit relatively normal growth and are fertile, with some phenotypes including defects in kidney development, postnatal thymic regeneration, and neurogenesis in the hippocampus (Qiao et al. 1999; Alpdogan et al. 2006; Terauchi et al. 2010; Lee et al. 2012). No liver phenotype during development or in adulthood has been reported. In order to analyze the LPC response in *Fgf7* knockout mice, adult littermates of wild-type and knockout mice were fed a DDC-containing diet or subjected to BDL. We measured the degree of LPC activation by CK19 immunostaining and confirmed that CK19$^+$ LPC numbers were increased by DDC or BDL in the wild-type liver (Fig. 4A,H).

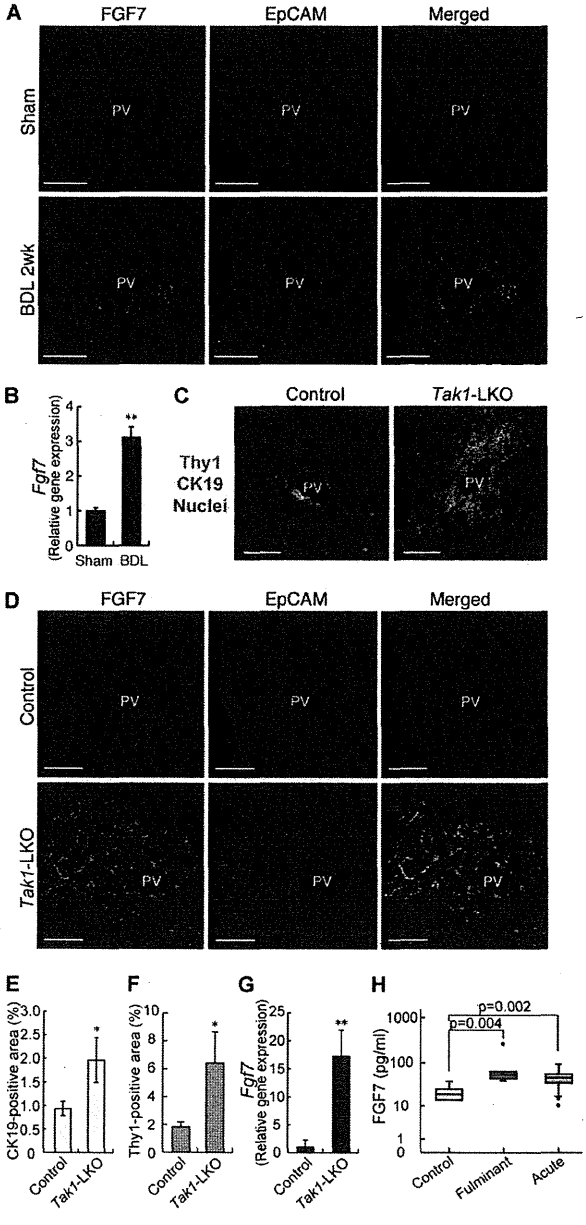

However, the LPC response was almost completely suppressed in *Fgf7* knockout mice (Fig. 4A,B,H,I). In contrast, quantitative analysis of the Thy1$^+$ area in *Fgf7* knockout mice revealed little change when compared with the wild-type control in both normal and damaged livers (Fig. 4C,J). In other words, Thy1$^+$ cells were capable of expanding in response to liver damage even in the absence of FGF7 function, consistent with the notion that FGF7 acts directly on LPCs rather than upstream of Thy1$^+$ cells. Ki67 or TUNEL staining with CK19 revealed that Ki67$^+$ proliferating cells among the CK19$^+$ LPCs were significantly decreased, although not completely abrogated, in the knockout mice compared with the wild-type control, while no statistically significant difference was observed in the TUNEL$^+$ cell population (Supplemental Fig. S7). These results suggest that the suppressed LPC response in *Fgf7* knockout mice can be attributed, at least in part, to reduced proliferation of LPCs rather than augmented induction of their apoptosis.

Fgf7 knockout mice were highly sensitive to DDC and had a low survival rate, whereas the wild-type mice were more resistant to hepatotoxin-induced liver injury (Fig. 4D). Upon DDC administration, systemic symptoms were obvious and generally more severe in the knockout than in the wild-type control, including jaundice, hemorrhagic diathesis, and weight loss, which are typically observed in end-stage liver disease (Figs. 4E,F; data not shown). Gross pathological and histopathological examinations of the mice that survived at 11 wk of injury confirmed that liver failure with severe leakage of bile into the liver vasculature is the most plausible cause of death in *Fgf7* knockout mice, while no fatal abnormality was recognized in any organs/tissues other than the liver (data not shown). We also performed serum biochemical tests using the mice fed DDC for 10 wk. The cholestasis markers total bilirubin (TBIL) and alkaline phosphatase (ALP) were both

Figure 3. FGF7-mediated LPC activation is conserved in several liver injuries. (*A*,*B*) Liver samples prepared from sham-operated (Sham) or BDL mice were subjected to the following experiments. (*A*) Confocal immunofluorescent double staining using anti-FGF7 (green) and anti-EpCAM (red) antibodies. Bars, 50 μm. (PV) Portal vein. (*B*) Quantitative RT–PCR analysis of *Fgf7* mRNA. Mean ± SE (n = 3). (**) $P < 0.01$. (*C–G*) Liver samples from 8-wk-old liver-specific *Tak1*-LKO (*Alfp-Cre*; *Tak1*$^{flox/flox}$) or control (*Tak1*$^{flox/flox}$) mice were subjected to the following experiments. (*C*) Representative images for immunofluorescent double staining of CK19 (red) and Thy1 (green). (PV) Portal vein. Bars, 80 μm. (*D*) Confocal immunofluorescent double staining using anti-FGF7 (green) and anti-EpCAM (red) antibodies. Bars, 50 μm. (PV) Portal vein. (*E*) Quantitative image analysis of CK19-positive area. Mean ± SD (n = 3). (*) $P < 0.05$. (*F*) Quantitative image analysis of Thy1-positive area. Mean ± SD (n = 3). (*) $P < 0.05$. (*G*) Quantitative RT–PCR analysis of *Fgf7* mRNA. Mean ± SD (n = 3). (**) $P < 0.01$. (*H*) Serum FGF7 levels in human samples. enzyme-linked immunosorbent assay (ELISA) for human FGF7 was performed on serum samples harvested from healthy controls (n = 6) and patients with fulminant (n = 6) or acute (n = 43) hepatitis. The data are presented as median (25–75 percentile).

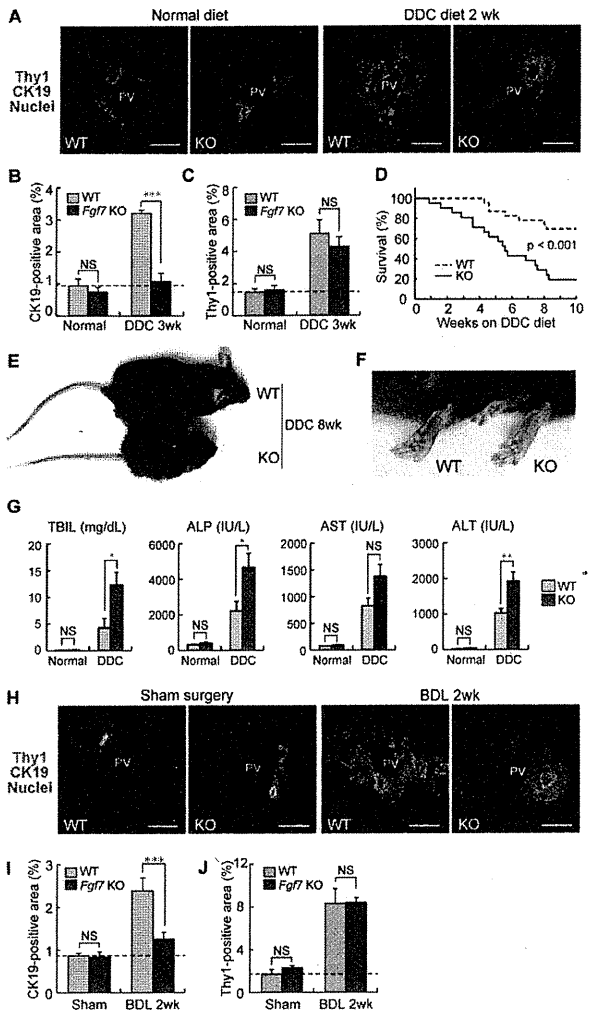

Figure 4. FGF7 is essential for LPC activation and liver regeneration in injured livers. Adult littermates of *Fgf7* knockout (KO) and wild-type (WT) mice were fed normal or DDC diet (*A–G*) or subjected to BDL or a sham operation (*H–J*). (*A,H*) Representative images for immunofluorescent double staining of CK19 (red) and Thy1 (green). Bars, 80 μm. (PV) Portal vein. (*B,I*) Quantitative image analysis of CK19-positive area. Mean ± SD ($n = 3$). (***) $P < 0.001$; (NS) not significant. (*C,J*) Quantitative image analysis of Thy1-positive area. Mean ± SD ($n = 3$). (NS) Not significant. (*D*) Kaplan-Meier survival curves of control (wild-type, $n = 23$) and *Fgf7* knockout ($n = 21$) mice given DDC, showing that the lack of FGF7 leads to the increased mortality after DDC feeding. Statistical analysis was performed using the log-rank (Mantel-Cox) test. (*E,F*) Appearance of *Fgf7* knockout and wild-type mice fed DDC diet for 8 wk. (*F*) More severe symptoms for jaundice, such as yellow-colored skin, were typically observed in the knockout animal. (*G*) Serum TBIL, ALP, AST, and ALT levels were measured in control and *Fgf7* knockout mice fed a normal (wild type, $n = 3$; knockout, $n = 3$) or DDC-containing (wild type, $n = 6$; knockout, $n = 3$) diet for 10 wk. Mean ± SE. (**) $P < 0.01$; (*) $P < 0.05$; (NS) not significant.

significantly increased in *Fgf7* knockout mice (Fig. 4G). At the same time, the level of the hepatocyte injury marker alanine transaminase (ALT) was significantly elevated in the knockout mice compared with the wild type, and that of aspartate transaminase (AST) also trended higher, but the difference was not statistically significant (Fig. 4G). At that point, the LPC numbers in the knockout mice could not keep up with those in wild-type mice (Supplemental Fig. S8A–C). These results indicate that the lack of FGF7 exacerbates damages in both hepatocytes and bile ducts and that the LPC response directly correlates with liver function and survival of an organism upon toxic insult. Taken together, we conclude that FGF7 is necessary for LPC activation in vivo at least in two different experimental models, and its expression and function may counter liver dysfunction.

Forced expression of FGF7 is sufficient to induce expansion of the LPC population in vivo

We next performed gain-of-function experiments to further explore the function of FGF7 in regulating the LPC response. First, we examined the effect of FGF7 on LPCs in vitro. We found that a recombinant FGF7 stimulated the proliferation of HSCE1, a cell line derived from EpCAM$^+$ LPCs of adult mice (Okabe et al. 2009), in a dose-dependent manner (Fig. 5A). To examine the effect of FGF7 in vivo, we used *Alfp-Cre; Rosa26-rtTA-IRES-EGFP; tetO-CMV-FGF7* triple Tg mice in which overexpression of FGF7 in the liver is achieved by doxycycline (Dox) treatment (Fig. 5B,C). A significant increase in CK19$^+$ LPC-like cell numbers was observed in the periportal regions of the triple Tg (hereafter referred to as *FGF7* Tg) mouse livers compared with control *Alfp-Cre; Rosa26-rtTA-IRES-EGFP* double Tg mouse livers (Figs. 5D,E). These expanding cells coexpressed other well-known LPC markers: A6, EpCAM, and SOX9 (Fig. 5E; Supplemental Fig. S9A,B). Notably, A6$^+$ CK19$^-$ cells, which can be regarded as a fraction of newly formed hepatocytes (Engelhardt et al. 1990; Ishikawa et al. 2012), were clearly detected adjacent to A6$^+$ CK19$^+$ LPCs in *FGF7* Tg mouse livers as well as in DDC-injured livers (Fig. 5D; Supplemental Fig. S6A), implying that the cell population induced by FGF7 has a potential to differentiate to hepatocytes.

Previous studies have shown that the extracellular matrix (ECM) plays an important role in regulating the LPC response and liver regeneration (Boulter et al. 2012; Español-Suñer et al. 2012). Immunostaining analysis of the type I and type III collagen proteins revealed that there was a significant accumulation of these ECM components around the expanding LPCs in response to FGF7 overexpression, similar to the case observed in the livers of DDC-treated animals (Fig. 5G). This strongly supports the notion that the FGF7-induced LPC induction in the normal liver faithfully recapitulates the phenomenon that occurs under the pathophysiological conditions in diseased livers. Meanwhile, the level of collagen gene expression (*Col1a1* and *Col3a1* for type I and type III collagens, respectively) using the whole-liver mRNA samples showed no significant increase in the expression of

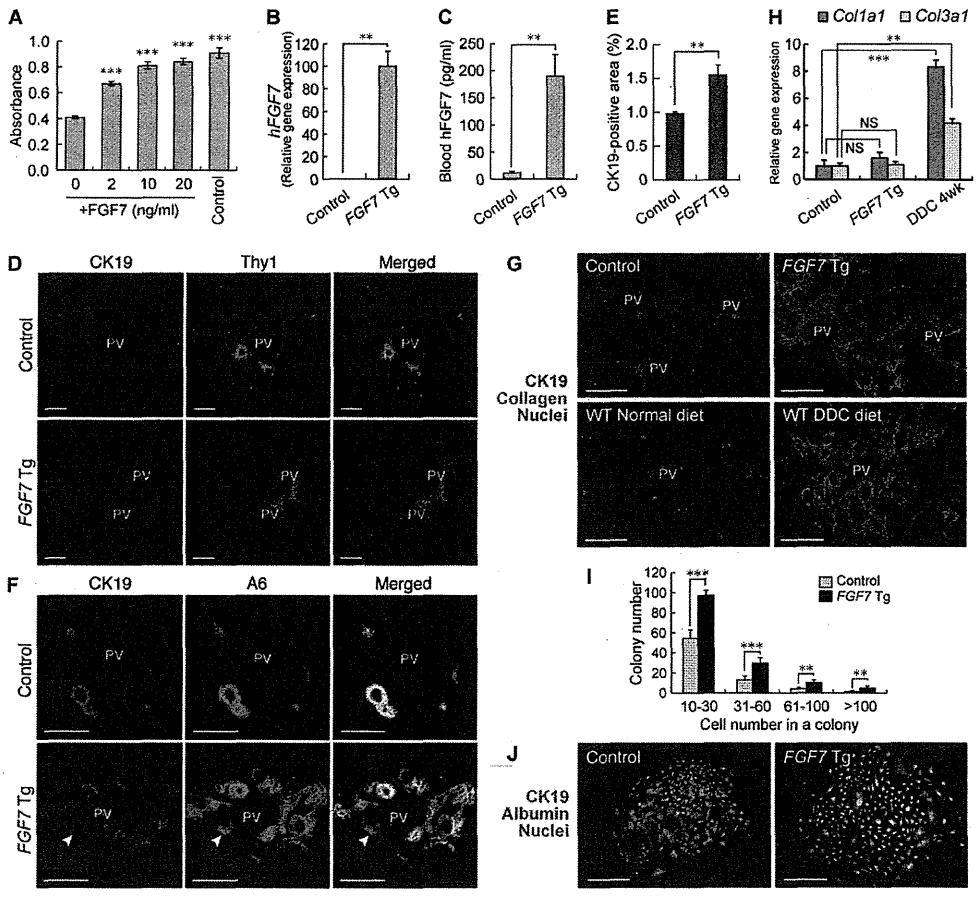

Figure 5. Overexpression of FGF7 can induce the LPC response in the adult mouse liver. (*A*) The level of proliferation of HSCE1 cells was examined by WST-1 assay. Stimulation with epidermal growth factor (EGF) and hepatocyte growth factor (HGF) was used as a control. Mean ± SD (n = 3). (***) $P < 0.001$ compared with no cytokine treatment (0). (*B*) Quantitative RT–PCR analysis was performed to assess human *FGF7* mRNA levels in the liver after 3 wk of Dox administration. Mean ± SE (control, n = 3; Tg, n = 5). (**) $P < 0.01$. (*C*) Serum levels of human FGF7 protein after 3 wk of Dox administration were determined by ELISA. Mean ± SE (control, n = 4; Tg, n = 6). (**) $P < 0.01$. (*D*) Immunostaining of CK19 (red) and Thy1 (green) in the livers of *FGF7* Tg mice and control mice treated with Dox for 4 wk. Bars, 100 μm. (PV) Portal vein. (*E*) Quantitative analysis of CK19-positive areas showed an increased number of LPC-like cells in *FGF7* Tg mice treated with Dox for 4 wk. Mean ± SD (n = 3). (**) $P < 0.01$. (*F*) Immunostaining of CK19 (red) and A6 (green) showed expansion of $CK19^+$ $A6^+$ LPCs in the livers of *FGF7* Tg mice treated with Dox for 4 wk. $CK19^-$ $A6^+$ newly formed hepatocytes were also observed (arrowheads). Bars, 50 μm. (PV) Portal vein. (*G*) Immunostaining of CK19 (red) and collagen (green) in the livers of *FGF7* Tg and control mice, wild-type mice fed a normal diet, and DDC-treated wild-type mice. Bars, 100 μm. (PV) Portal vein. (*H*) Quantitative RT–PCR analysis of *Col1a1* and *Col3a1* mRNA. Mean ± SE (control, n = 3; Tg, n = 5; DDC, n = 3). (**) $P < 0.01$; (***) $P < 0.001$; (NS) not significant. (*I*) $EpCAM^+$ cells were isolated from the livers of *FGF7* Tg mice and control mice 3 wk after Dox treatment and subjected to the in vitro colony formation assay. Mean ± SD (n = 3). (**) $P < 0.01$; (***) $P < 0.001$. (*J*) Immunofluorescence images of representative large colonies stained with anti-CK19 (green) and albumin (red). Bars, 200 μm.

either of these genes at the whole-organ level (Fig. 5H). Thus, overexpression of FGF7 in the liver results in local deposition of ECMs associated with the LPC expansion but does not lead to a global fibrogenic response in the organ.

To further characterize the FGF7-induced LPC-like population in terms of functional criteria, we next performed clonogenic assays to evaluate its proliferative and bilineage differentiation potentials in vitro. It has been well documented that stem/progenitor cell activity of a certain population of liver cells can be defined by their capacity to generate large colonies that are capable of expressing both hepatocyte and BEC lineage markers in culture (Suzuki et al. 2008; Okabe et al. 2009; Dorrell et al. 2011; Shin et al. 2011). When $EpCAM^+$ cells isolated from the *FGF7* Tg mice and the control mice were subjected to in vitro colony formation assays (Okabe et al. 2009), the $EpCAM^+$ cells from the Tg mice formed colonies, including those composed of >100 cells (Fig. 5I). Immunostaining analyses confirmed that these large colonies were composed of both albumin-positive (the hepatocyte marker) and CK19-positive (the LPC/BEC marker)

cells, indicative of the bilineage differentiation in vitro (Fig. 5J). Most importantly, the colony-forming rate for both large and smaller colonies was significantly increased in the *FGF7* Tg mice. Thus, overexpression of FGF7 in vivo in the mouse liver leads to expansion of LPCs that are characterized by LPC marker expressions as well as clonogenicity and bipotency in vitro. Taken together, we conclude that FGF7 alone is sufficient to generate a population of cells that are phenotypically and functionally indistinguishable from LPCs.

Overexpression of FGF7 reverses both the hepatocyte damage and cholestatic liver injury

Given the potent activity of FGF7 in promoting the LPC response, we reasoned that application of this molecule should exert some protective effect on the liver against toxic insults. To test this possibility, the Tg mouse system was used to start ectopic FGF7 expression by Dox administration 1 wk after the onset of the course of DDC-induced chronic liver injury (Fig. 6A). Under this condition, increases in the level of the cholestatic markers TBIL and ALP were greatly reduced in *FGF7* Tg mice compared with the control mice, with the severity of symptoms of jaundice being apparently reduced, which means that bile duct obstruction was alleviated (Fig. 6B,C). At the same time, the levels of AST and ALT were also significantly improved in *FGF7* Tg mice, indicating less hepatocyte injury by overexpression of FGF7 (Fig. 6C). To further substantiate the notion that FGF7 does not simply prevent the damage but rather reverses and improves the symptoms of well-established chronic liver failure, we performed similar experiments by starting Dox administration to induce *FGF7* expression in the liver 3 wk after the onset of the DDC administration (Supplemental Fig. S10A,B). Again, serum biochemical analyses showed decreased levels of both hepatocyte injury and cholestasis markers, although the difference was not statistically significant with regard to ALP (Supplemental Fig. S10C). These data suggest that the severity of the damage on both hepatocytes and BECs can be relieved by an excess of FGF7 through the activation of LPCs that are bipotential and hence capable of contributing to the recovery of both lineages.

Histochemical examination revealed that deposition of brown pigment plugs derived from porphyrin crystals, a hallmark of the DDC-injured liver, was decreased in the Tg liver (Fig. 6D). Single-cell necrosis was reduced in

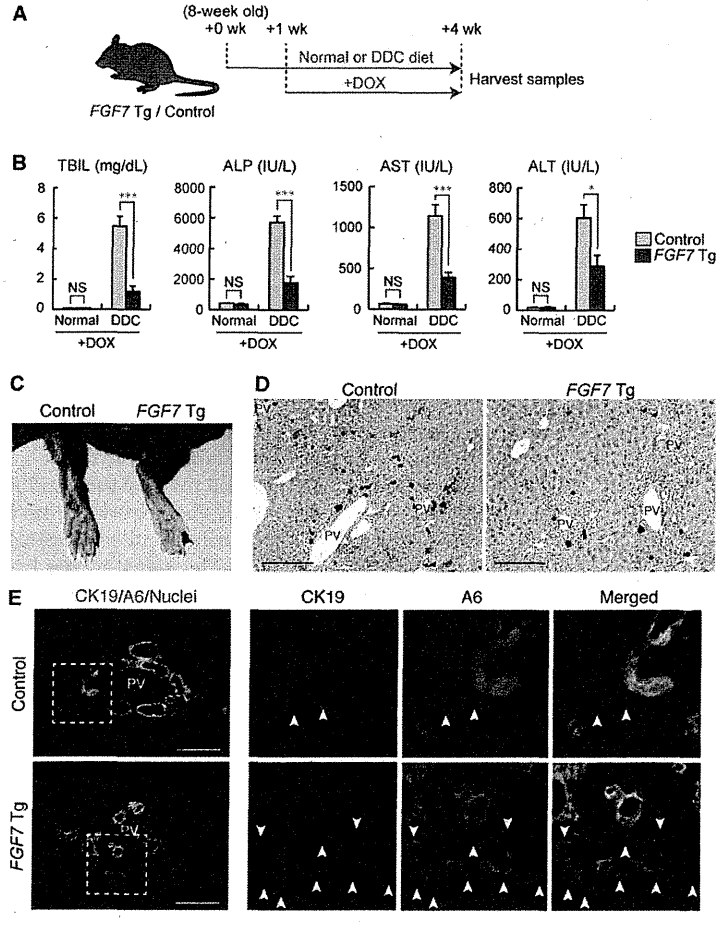

Figure 6. Application of FGF7 improves both the hepatocyte damage and cholestatic liver injury. (*A*) Schematic representation of the experiment. Eight-week-old *FGF7* Tg and control mice were subjected to the DDC-induced liver injury model or left untreated, and 1 wk later, Dox administration was started for FGF7 induction. After 3 wk of treatment, serum and liver samples were harvested for subsequent analyses. (*B*) Serum TBIL, ALP, AST, and ALT levels were measured in control and *FGF7* Tg mice fed a normal (control, $n = 3$; Tg, $n = 3$) or DDC-containing (control, $n = 9$; Tg, $n = 7$) diet. Mean ± SE. (***) $P < 0.001$; (*) $P < 0.05$; (NS) not significant. (*C*) Typical skin color (*right* foot) of the DDC-treated animals at the end of the protocol, indicating that *FGF7* Tg mice suffered less from jaundice than control mice. (*D*) Hematoxylin and eosin staining of livers from DDC-treated animals at the end of the protocol. Bars, 200 μm. (PV) Portal vein. (*E*) Immunostaining of CK19 (red) and A6 (green) in the livers of FGF7 Tg mice and control mice at the end of the protocol. Note that $A6^+$ $CK19^-$ newly formed hepatocytes were increased in the livers of *FGF7* Tg mice. Bars, 100 μm. (PV) Portal vein.

some of the Tg mice compared with the control (data not shown). In the case of the mice fed DDC for 6 wk, some morphological changes associated with the reacting ductules were observed in the Tg mice, including thickened epithelial layers and more dilated luminal structures (Supplemental Fig. S10D,E). Most remarkably, immunostaining analyses revealed that $A6^+$ $CK19^-$ newly formed hepatocytes were dramatically increased around the expanding $A6^+$ $CK19^+$ LPCs (Figs. 6E; Supplemental Fig. S10E). This strongly suggests that overexpression of FGF7 contributes to parenchymal regeneration by accelerating differentiation and production of hepatocytes from LPCs in the DDC-induced liver injury model. In conclusion, our results indicate that FGF7 secreted by $Thy1^+$ cells mediates the activation of adult LPCs as a niche signal and promotes progenitor cell-dependent liver regeneration (Fig. 7).

Discussion

In this study, we demonstrate that FGF7 plays a critical role in inducing LPCs and that the LPC response contributes to survival in severe liver injury. From the standpoint of adult tissue stem/progenitor cells, this study has substantiated the concept of the niche for LPCs in the regenerating liver by molecular characterization.

In general, tissue stem/progenitor cells are supported and regulated by their surrounding microenvironment or the stem cell niche. While several secreted molecules that participate in the LPC response have been reported (Erker and Grompe 2007), their possible involvement as niche signals has not been explored. This study provides compelling evidence that $Thy1^+$ periportal cells form the niche for LPCs by residing in close proximity to LPCs and producing a key regulatory factor, FGF7. Since FGF7-producing $Thy1^+$ cells express markers for portal fibroblasts, hepatic stellate cells, and myofibroblast, we consider that $Thy1^+$ cells are a heterogeneous population of mesenchymal cells. Our data are consistent with a previous report that hepatic stellate cells express FGF7 in chronic liver disease (Steiling et al. 2004). Although further characterization of the $Thy1^+$ cells is needed to give a clear definition of the LPC niche, we hereby propose that the stem cell niche is present in the adult liver under the regenerating conditions. It has been reported that $Thy1^+$ cells are also observed in the livers of patients with fulminant liver failure accompanying the LPC response (Dezso et al. 2007). In addition, high expression of FGF7 in patients with chronic liver diseases (Steiling et al. 2004; Otte et al. 2007) and in experimental rat models of hepatic fibrosis (Murakami et al. 2011) were previously reported. Thus, we predict that LPCs are regulated through the same mechanism in humans as in rodents.

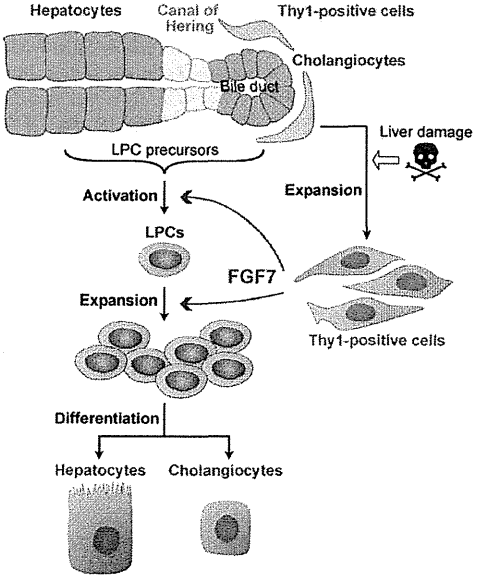

Figure 7. A model for regulatory mechanism of the LPC response by FGF7. In injured livers, $Thy1^+$ mesenchymal cells expand in the periportal area and produce FGF7. FGF7 contributes to liver regeneration by initiating the activation and proliferation of LPCs as the functional niche signal.

The LPC response is a complicated physiological response to liver injuries involving several kinds of cells, such as hepatocytes, BECs, immune cells, hepatic stellate cells, and portal fibroblasts. We demonstrated that FGF7 is both necessary and sufficient for its induction. To our knowledge, this is the first study to prove that FGF signaling is involved in LPC regulation. Upstream and downstream signaling events of FGF7 need to be explored to further elucidate the regulatory mechanism of LPCs. Previous studies have identified TNF (tumor necrosis factor)-like weak inducer of apoptosis (Tweak) as a mitogen for LPCs (Jakubowski et al. 2005; Tirnitz-Parker et al. 2010). Tweak is a member of the TNF family and binds to the FGF-inducible 14-kDa protein (Fn14) receptor (Meighan-Mantha et al. 1999). Although the LPC response in *Fn14* knockout mice was attenuated after 2 wk of CDE treatment, it was restored later and eventually resulted in a level equivalent to that in wild-type mice (Tirnitz-Parker et al. 2010). In contrast, we showed in this study that LPC activation was not sufficiently induced in *Fgf7* knockout mice even after long-term liver injury. Thus, the role of FGF7 signal may be more direct and indispensable in LPC induction, while that of the Tweak/Fn14 pathway may be rather enhancing and not necessarily required. Recently, hepatocyte growth factor (HGF)/c-Met signaling has been reported to play a necessary role in LPC-mediated liver regeneration in the mouse DDC diet model (Ishikawa et al. 2012), although it remains unexplored whether it can also be sufficient to induce the LPC response, as is the case with FGF7. The relationship between FGF7 and these signaling pathways is an important issue to be addressed. In addition, recent studies have suggested that the cellular and molecular mechanisms underlying the injury/regeneration processes in the DDC injury are apparently different from the CDE regimen, another well-appreciated model to study LPCs (Boulter et al. 2012; Español-Suñer et al. 2012). It should be determined whether and how FGF7 is involved in the latter case.

We showed that forced expression of FGF7 in hepatocytes induces the LPC response in the normal liver. Intriguingly, induced LPC-like cells were observed only in the periportal area despite global expression of FGF7 within the liver. As the LPC response upon liver injury also takes place in the periportal region, FGF7-induced LPC-like cells may be derived from the genuine origin and undergo the normal ontogeny of LPCs. The origin of LPCs is still under debate. The canals of Hering that connect bile ducts to hepatocytes have long been considered a promising candidate (Paku et al. 2001); however, direct proof of this idea has been hampered by the lack of a specific molecular marker for these cells. BECs are phenotypically quite similar to LPCs and can thus be a likely candidate (Alison et al. 1996; Okabe et al. 2009). Indeed, recent studies using a genetic lineage tracing system based on *Sox9-CreERT2* mouse lines have suggested this possibility (Dorrell et al. 2011; Furuyama et al. 2011), although the nature of the Sox9-expressing cells should be further evaluated and rigorously determined with considerable caution (Carpentier et al. 2011). At the same time, hepatocytes have also been considered as possible LPC precursors, as they can be converted to BEC- or LPC-like cells under certain circumstances (Michalopoulos et al. 2005; Nishikawa et al. 2005; Zong et al. 2009). With regard to this notion, it should be noted that while FGFR2b is highly expressed in LPCs, it is also weakly but certainly expressed in the hepatocyte fraction. Considering the heterogeneity of hepatocytes, it is worthwhile to explore the nature of LPC precursors based on the expression pattern of FGFR2b. It is also possible that the local environmental cues, such as ECMs, in the periportal region participate in dictating the competence of LPC precursors for activation by FGF7, leading to a spatially stereotyped induction pattern of the LPC response.

While it has long been documented that LPCs appear and proliferate in injured and cancerous livers, whether LPCs participate in regeneration has not been clear to date. Our data, based on loss-of-function and gain-of-function experiments with FGF7, demonstrate that the level of LPC activation correlates with resilience and survival in cases of severe liver injury and suggest that LPCs practically contribute to liver regeneration. It is formally not excluded that FGF7 may act directly on damaged hepatocytes and/or BECs to cause some protective effects, and further analyses will be required to discriminate these possibilities. In either case, FGF7 can be regarded as a highly effective molecule to reverse liver damage. It has been reported that application of recombinant FGF7 protein in mice results in enhanced expression of detoxifying enzymes in the liver, while mice lacking both FGFR1 and FGFR2 in hepatocytes show increased mortality after PHx with impaired expression of those enzymes (Böhm et al. 2010). PHx has generally been regarded as the model for liver regeneration achieved by compensatory proliferation of hepatocytes rather than by LPCs, but several recent studies have implicated a possible involvement of the latter as well (Furuyama et al. 2011; Iverson et al. 2011; Malato et al. 2011). Although the study by Böhm et al. (2010) did not mean to address the role of endogenous FGF7, it would be worth exploring whether the potential beneficial effect of FGF7 observed therein is attributable to ectopic activation of LPCs. An N-terminally truncated form of FGF7, palifermin, has already been approved for the treatment of chemoradiation-induced oral mucositis (Beaven and Shea 2007). In spite of the ability of this drug to improve wound healing responses, its potential for therapeutic application to human liver diseases has not been tested. Our present study provides evidence that FGF7 or its derivatives may have clinical implications for patients with hepatic dysfunction as well.

Materials and methods

Animals

Fgf7 knockout mice (Guo et al. 1996) were obtained from The Jackson Laboratory. All of the experiments in this study were performed on littermates derived from the mating of heterozygotes. In order to generate liver-specific *Tak1*-deficient mice (*Tak1*-LKO mice), mice carrying floxed alleles of the *Tak1* gene (*Tak1*$^{flox/flox}$) (Sato et al. 2005), maintained by and obtained from JCRB (Japanese Collection of Research Bioresources Cell Bank) Laboratory Animal Resource Bank, NIBIO (National Institute of Biomedical Innovation, Osaka), were crossed with *Alfp-Cre* Tg mice (kindly provided by Dr. Klaus Kaestner, University of Pennsylvania) (Zhang et al. 2005). For the *FGF7* Tg mouse line in which human FGF7 is overexpressed in the liver upon treatment with Dox, the *Alfp-Cre* Tg mice, *ROSA26-rtTA-IRES-EGFP* knock-in mice (obtained from The Jackson Laboratory) (Belteki et al. 2005), and *tetO-CMV-FGF7* Tg mice (kindly provided by Dr. Jeffrey A. Whitsett, Cincinnati Children's Hospital Medical Center) (Tichelaar et al. 2000) were crossed to prepare *Alfp-Cre; rtTA/+; FGF7* triple Tg mice. Littermates lacking the *FGF7* transgene (*Alfp-Cre; rtTA/+*) were used as a control. Dox was administrated in drinking water (2 g/L) supplemented with 1% sucrose. For lineage tracing experiments, the *Alfp-Cre* Tg mice were crossed with the *R26R-EYFP* reporter strain (Srinivas et al. 2001). Wild-type C57BL/6J mice were purchased from CLEA Japan, Inc. All animals were maintained under standard SPF conditions. The experiments were performed according to the guideline set by the institutional animal care and use committee of the University of Tokyo. Mouse LPCs were activated by feeding with a 0.1% DDC-containing diet (F-4643, Bio-serv) or common BDL using a standard technique.

Antibodies

For immunohistochemistry, rat monoclonal antibodies against mouse EpCAM (used at a dilution of 1:200; 552370) and Thy1 (1:200; 553011) were purchased from BD Bioscience. The goat anti-mouse albumin (1:100; A90-234A, Bethyl Laboratories), rabbit anti-Desmin (1:400; ab8592, Abcam), rabbit anti-rat Elastin (1:100; CL55041AP, Cedarlane), rabbit anti-GFP (1:50; G10362, Life Technologies), rabbit anti-human Ki67 (1:200; NCL-Ki67p, Leica), and rabbit anti-Sox9 (1:1000; AB5535, Millipore) antibodies were also commercially obtained and used. A mixture of rabbit anti-collagen type I (1:100; 2150-1410, AbD serotec) and rabbit anti-collagen type III (1:300; ab7778, Abcam) was used to detect collagen fibers. The rat anti-mouse CK19 (TROMA-III) was obtained from the Developmental Studies Hybridoma Bank and used at 250 ng/mL. The rabbit anti-mouse CK19 antibody (1:1000–1:2000) was raised as previously described (Tanimizu

et al. 2003). The rabbit anti-FGF7 (1:100) and anti-FGFR2b (1:200) antibodies were as described (Yamamoto-Fukuda et al. 2003). The A6 antibody (1:10–1:20) was a generous gift from Dr. Valentina Factor (National Institutes of Health). For flow cytometry, the rat anti-EpCAM monoclonal antibody (1:500) was raised as described previously (Okabe et al. 2009). The rat anti-mouse CD45 APC antibody (1:100; 30-F11) was purchased from BD Bioscience. The anti-Thy1 antibody was the same as described above.

Histological analysis

Frozen sections (8 μm) from the liver were placed on APS-coated glass slides (Matsunami Glass) using a HM505E cryostat (Microm International). After blocking in 5% skim milk/PBS, the samples were incubated with primary antibodies and then with fluorescence-conjugated secondary antibodies. Nuclei were counterstained with Hoechst 33342 (Sigma). Liver sections were imaged with fluorescence microscopes (Axioskop 2 plus and Axio Observer.Z1, Zeiss) or a confocal microscope (Fluoview FV1000, Olympus). For the quantification of positive areas, immunostained liver sections were imaged and quantified using an In Cell Analyzer 2000 (GE Healthcare). TUNEL assay was performed using the In Situ Apoptosis Detection kit (MK500, TaKaRa) according to the manufacturer's instructions. Gross pathological and histopathological examinations of *Fgf7* knockout and control mice were performed by BOZO Research Center, Inc.

Section in situ hybridization analysis

Paraffin sections were prepared from liver specimens, and a digoxigenin-labeled antisense RNA probe for mouse *Fgfr2* was used for in situ hybridization by the method of Genostaff, Inc. The probe sequence is shown in Supplemental Table S2, and the hybridization conditions are available on request. After images for in situ hybridization staining were obtained, the sections were further processed for immunohistochemical staining with the anti-CK19 antibody. The same fields of view as in in situ hybridization were chosen and photographed.

Cell preparation and flow cytometry

A single-cell suspension from the liver was obtained by a two-step collagenase perfusion method as described previously (Okabe et al. 2009). In short, liver specimens were perfused with basic perfusion solution containing 0.5 g/L collagenase type IV (Sigma). The undigested clot was redigested with basic perfusion solution containing 0.5 g/L collagenase type IV, 0.5 g/L pronase (Roche), and 50 mg/L DNaseI (Sigma). This digested liver was passed through a 70-μm cell strainer. After centrifugation at 700 rpm for 2 min, the pellet was used for separation of hepatocytes by Percoll density centrifugation. The supernatant was transferred to a new tube and centrifuged repeatedly until no pellet was visible. The final supernatant was centrifuged at 1200 rpm for 5 min, and the precipitated cells were used as NPCs for flow cytometry. Aliquots of cells were blocked with anti-FcR antibody, costained with fluorescence- and/or biotin-conjugated antibodies, and then incubated with PE-conjugated streptavidin (BD Biosciences) if needed. The samples were analyzed by FACSCalibur (Becton Dickinson) or sorted by Moflo XDP (Beckman-Coulter). Dead cells were excluded by propidium iodide staining.

Quantitative RT–PCR

Total RNA was isolated from whole-liver samples or sorted cell populations using Trizol reagent (Invitrogen) and treated with DNaseI (Invitrogen). Total RNA and random hexamer primers were used for cDNA synthesis with SuperScript III (Invitrogen) or High-Capacity cDNA Reverse Transcription kit (Applied Biosystems). Quantitative RT–PCR analyses were performed using LightCycler (Roche) with SYBR Premix Ex Taq (Takara). *Gapdh* was used as an internal control. Primer sequences are listed in Supplemental Table S1.

Cell culture and proliferation assay

The hepatic progenitor cell line HSCE1 was established and characterized as described previously (Okabe et al. 2009). HSCE1 cells were maintained in type I collagen-coated dishes using a medium supplemented with fetal bovine serum and 10 ng/mL each recombinant human EGF and HGF. The proliferative response of HSCE1 cells was examined in the absence of the serum by a colorimetric assay using WST-1 cell proliferation reagent (Roche) according to the manufacturer's directions. The absorbance value (OD450-OD650) was measured using an Emax microplate reader (Molecular Devices).

In vitro colony formation assay

$EpCAM^+$ cells were sorted as described previously (Okabe et al. 2009) and plated at 5×10^3 cells per 35-mm dish. The cells were cultured for 9 d, and then the number and size of colonies were counted.

Human FGF7 immunoassay

Human FGF7 concentration in serum was quantitatively determined in duplicate by FGF7-specific enzyme-linked immunosorbent assay (ELISA; R&D systems, Inc.) according to the manufacturer's instructions. In brief, FGF7 standards and samples were placed in the provided monoclonal antibody-coated microplates. After the reaction, an enzyme-linked polyclonal antibody specific for FGF7 was added and incubated for 2 h at room temperature. The unbound components were washed off at each step, whereas bound FGF7 was determined by ELISA reader (Immunomini NJ2300, Cosmo Bio Co., Ltd.). Statistical analysis in Figure 3H was carried out using a Kruskal-Wallis test and a Mann-Whitney test in SPSS Statistics 17.0 software. The study protocol conformed to the ethical guidelines of the 1975 Declaration of Helsinki and was approved by the ethics committees of Iwate Medical University and The University of Tokyo. Informed consent was obtained from all patients.

Statistical analysis

Data were analyzed and statistics were performed using unpaired two-tailed Student's *t*-test unless otherwise indicated. Comparisons of gene expression in multiple liver cell fractions (Fig. 2D; Supplemental Figs. S4A, S5, S6) were done using one-way analysis of variance (ANOVA) with subsequent Tukey tests. $P < 0.05$ was considered statistically significant.

Acknowledgments

We thank Dr. K. Kaestner, Dr. J.A. Whitsett, and JCRB Laboratory Animal Resource Bank at NIBIO for providing mouse strains; Dr. V. Factor for an antibody; H. Bae, Y. Kamiya, A. Kikuchi, N. Miyata, S. Saito, and H. Sato for technical assistance; and the members of the Miyajima laboratory for discussions and suggestions. The TROMA-III developed by Dr. Rolf Kemler was obtained from the Developmental Studies Hybridoma Bank developed under the auspices of the NICHD and maintained by the Department of Biology at The University of Iowa. This

work was supported by research grants from the Ministry of Education, Culture, Sports, Science, and Technology of Japan (to T.I. and A.M.); Ministry of Health, Labor, and Welfare of Japan (to A.M.); the CREST program from Japan Science and Technology Agency (to A.M.); and the Takeda Science Foundation (to A.M.). H.M.T. was a Research Fellow of the Japan Society for the Promotion of Science.

References

Akhurst B, Croager EJ, Farley-Roche CA, Ong JK, Dumble ML, Knight B, Yeoh GC. 2001. A modified choline-deficient, ethionine-supplemented diet protocol effectively induces oval cells in mouse liver. *Hepatology* **34:** 519–522.

Alison MR, Golding MH, Sarraf CE. 1996. Pluripotential liver stem cells: Facultative stem cells located in the biliary tree. *Cell Prolif* **29:** 373–402.

Alpdogan O, Hubbard VM, Smith OM, Patel N, Lu S, Goldberg GL, Gray DH, Feinman J, Kochman AA, Eng JM, et al. 2006. Keratinocyte growth factor (KGF) is required for postnatal thymic regeneration. *Blood* **107:** 2453–2460.

Beaven AW, Shea TC. 2007. The effect of palifermin on chemotherapyand radiation therapy-induced mucositis: A review of the current literature. *Support Cancer Ther* **4:** 188–197.

Beer HD, Bittner M, Niklaus G, Munding C, Max N, Goppelt A, Werner S. 2005. The fibroblast growth factor binding protein is a novel interaction partner of FGF-7, FGF-10 and FGF-22 and regulates FGF activity: Implications for epithelial repair. *Oncogene* **24:** 5269–5277.

Belteki G, Haigh J, Kabacs N, Haigh K, Sison K, Costantini F, Whitsett J, Quaggin SE, Nagy A. 2005. Conditional and inducible transgene expression in mice through the combinatorial use of Cre-mediated recombination and tetracycline induction. *Nucleic Acids Res* **33:** e51.

Bettermann K, Vucur M, Haybaeck J, Koppe C, Janssen J, Heymann F, Weber A, Weiskirchen R, Liedtke C, Gassler N, et al. 2010. TAK1 suppresses a NEMO-dependent but NF-κB-independent pathway to liver cancer. *Cancer Cell* **17:** 481–496.

Bird TG, Lorenzini S, Forbes SJ. 2008. Activation of stem cells in hepatic diseases. *Cell Tissue Res* **331:** 283–300.

Böhm F, Speicher T, Hellerbrand C, Dickson C, Partanen JM, Ornitz DM, Werner S. 2010. FGF receptors 1 and 2 control chemically induced injury and compound detoxification in regenerating livers of mice. *Gastroenterology* **139:** 1385–1396.

Boulter L, Govaere O, Bird TG, Radulescu S, Ramachandran P, Pellicoro A, Ridgway RA, Seo SS, Spee B, Van Rooijen N, et al. 2012. Macrophage-derived Wnt opposes Notch signaling to specify hepatic progenitor cell fate in chronic liver disease. *Nat Med* **18:** 572–579.

Carpentier R, Suñer RE, van Hul N, Kopp JL, Beaudry JB, Cordi S, Antoniou A, Raynaud P, Lepreux S, Jacquemin P, et al. 2011. Embryonic ductal plate cells give rise to cholangiocytes, periportal hepatocytes, and adult liver progenitor cells. *Gastroenterology* **141:** 1432–1438.

Dezso K, Jelnes P, Laszlo V, Baghy K, Bodor C, Paku S, Tygstrup N, Bisgaard HC, Nagy P. 2007. Thy-1 is expressed in hepatic myofibroblasts and not oval cells in stem cell-mediated liver regeneration. *Am J Pathol* **171:** 1529–1537.

Dorrell C, Erker L, Schug J, Kopp JL, Canaday PS, Fox AJ, Smirnova O, Duncan AW, Finegold MJ, Sander M, et al. 2011. Prospective isolation of a bipotential clonogenic liver progenitor cell in adult mice. *Genes Dev* **25:** 1193–1203.

Duncan AW, Dorrell C, Grompe M. 2009. Stem cells and liver regeneration. *Gastroenterology* **137:** 466–481.

Engelhardt NV, Factor VM, Yasova AK, Poltoranina VS, Baranov VN, Lasareva MN. 1990. Common antigens of mouse oval and biliary epithelial cells. Expression on newly formed hepatocytes. *Differentiation* **45:** 29–37.

Erker L, Grompe M. 2007. Signaling networks in hepatic oval cell activation. *Stem Cell Res* **1:** 90–102.

Español-Suñer R, Carpentier R, Van Hul N, Legry V, Achouri Y, Cordi S, Jacquemin P, Lemaigre F, Leclercq IA. 2012. Liver progenitor cells yield functional hepatocytes in response to chronic liver injury in mice. *Gastroenterology* **143:** 1564–1575.

Farber E. 1956. Similarities in the sequence of early histological changes induced in the liver of the rat by ethionine, 2-acetylamino-fluorene, and 3'-methyl-4-dimethylaminoazobenzene. *Cancer Res* **16:** 142–148.

Fausto N. 2004. Liver regeneration and repair: Hepatocytes, progenitor cells, and stem cells. *Hepatology* **39:** 1477–1487.

Furuyama K, Kawaguchi Y, Akiyama H, Horiguchi M, Kodama S, Kuhara T, Hosokawa S, Elbahrawy A, Soeda T, Koizumi M, et al. 2011. Continuous cell supply from a Sox9-expressing progenitor zone in adult liver, exocrine pancreas and intestine. *Nat Genet* **43:** 34–41.

Gerhart J. 1999. 1998 Warkany lecture: Signaling pathways in development. *Teratology* **60:** 226–239.

Guo L, Degenstein L, Fuchs E. 1996. Keratinocyte growth factor is required for hair development but not for wound healing. *Genes Dev* **10:** 165–175.

Inokuchi S, Aoyama T, Miura K, Osterreicher CH, Kodama Y, Miyai K, Akira S, Brenner DA, Seki E. 2010. Disruption of TAK1 in hepatocytes causes hepatic injury, inflammation, fibrosis, and carcinogenesis. *Proc Natl Acad Sci* **107:** 844–849.

Ishikawa T, Factor VM, Marquardt JU, Raggi C, Seo D, Kitade M, Conner EA, Thorgeirsson SS. 2012. Hepatocyte growth factor/c-met signaling is required for stem-cell-mediated liver regeneration in mice. *Hepatology* **55:** 1215–1226.

Itoh N, Ornitz DM. 2008. Functional evolutionary history of the mouse Fgf gene family. *Dev Dyn* **237:** 18–27.

Iverson SV, Comstock KM, Kundert JA, Schmidt EE. 2011. Contributions of new hepatocyte lineages to liver growth, maintenance, and regeneration in mice. *Hepatology* **54:** 655–663.

Jakubowski A, Ambrose C, Parr M, Lincecum JM, Wang MZ, Zheng TS, Browning B, Michaelson JS, Baetscher M, Wang B, et al. 2005. TWEAK induces liver progenitor cell proliferation. *J Clin Invest* **115:** 2330–2340.

Knight B, Matthews VB, Olynyk JK, Yeoh GC. 2005. Jekyll and Hyde: Evolving perspectives on the function and potential of the adult liver progenitor (oval) cell. *Bioessays* **27:** 1192–1202.

Knight B, Akhurst B, Matthews VB, Ruddell RG, Ramm GA, Abraham LJ, Olynyk JK, Yeoh GC. 2007. Attenuated liver progenitor (oval) cell and fibrogenic responses to the choline deficient, ethionine supplemented diet in the BALB/c inbred strain of mice. *J Hepatol* **46:** 134–141.

Lee CH, Javed D, Althaus AL, Parent JM, Umemori H. 2012. Neurogenesis is enhanced and mossy fiber sprouting arises in FGF7-deficient mice during development. *Mol Cell Neurosci* **51:** 61–67.

Libbrecht L, Roskams T. 2002. Hepatic progenitor cells in human liver diseases. *Semin Cell Dev Biol* **13:** 389–396.

Liu XH, Aigner A, Wellstein A, Ray PE. 2001. Up-regulation of a fibroblast growth factor binding protein in children with renal diseases. *Kidney Int* **59:** 1717–1728.

Lowes KN, Brennan BA, Yeoh GC, Olynyk JK. 1999. Oval cell numbers in human chronic liver diseases are directly related to disease severity. *Am J Pathol* **154:** 537–541.

Lu J, Izvolsky KI, Qian J, Cardoso WV. 2005. Identification of FGF10 targets in the embryonic lung epithelium during bud morphogenesis. *J Biol Chem* **280:** 4834–4841.

Malato Y, Naqvi S, Schürmann N, Ng R, Wang B, Zape J, Kay MA, Grimm D, Willenbring H. 2011. Fate tracing of mature hepatocytes in mouse liver homeostasis and regeneration. *J Clin Invest* **121:** 4850–4860.

Meighan-Mantha RL, Hsu DK, Guo Y, Brown SA, Feng SL, Peifley KA, Alberts GF, Copeland NG, Gilbert DJ, Jenkins NA, et al. 1999. The mitogen-inducible Fn14 gene encodes a type I transmembrane protein that modulates fibroblast adhesion and migration. *J Biol Chem* **274:** 33166–33176.

Michalopoulos GK, DeFrances MC. 1997. Liver regeneration. *Science* **276:** 60–66.

Michalopoulos GK, Barua L, Bowen WC. 2005. Transdifferentiation of rat hepatocytes into biliary cells after bile duct ligation and toxic biliary injury. *Hepatology* **41:** 535–544.

Murakami KI, Kaji T, Shimono R, Hayashida Y, Matsufuji H, Tsuyama S, Maezono R, Kosai KI, Takamatsu H. 2011. Therapeutic effects of vitamin A on experimental cholestatic rats with hepatic fibrosis. *Pediatr Surg Int* **27:** 863–870.

Nishikawa Y, Doi Y, Watanabe H, Tokairin T, Omori Y, Su M, Yoshioka T, Enomoto K. 2005. Transdifferentiation of mature rat hepatocytes into bile duct-like cells in vitro. *Am J Pathol* **166:** 1077–1088.

Okabe M, Tsukahara Y, Tanaka M, Suzuki K, Saito S, Kamiya Y, Tsujimura T, Nakamura K, Miyajima A. 2009. Potential hepatic stem cells reside in $EpCAM^+$ cells of normal and injured mouse liver. *Development* **136:** 1951–1960.

Otte JM, Schwenger M, Brunke G, Schmitz F, Otte C, Kiehne K, Kloehn S, Monig H, Schmidt WE, Herzig KH. 2007. Differential regulated expression of keratinocyte growth factor and its receptor in experimental and human liver fibrosis. *Regul Pept* **144:** 82–90.

Paku S, Schnur J, Nagy P, Thorgeirsson SS. 2001. Origin and structural evolution of the early proliferating oval cells in rat liver. *Am J Pathol* **158:** 1313–1323.

Ponder KP. 1996. Analysis of liver development, regeneration, and carcinogenesis by genetic marking studies. *FASEB J* **10:** 673–682.

Preisegger KH, Factor VM, Fuchsbichler A, Stumptner C, Denk H, Thorgeirsson SS. 1999. Atypical ductular proliferation and its inhibition by transforming growth factor β1 in the 3,5-diethoxycarbonyl-1,4-dihydrocollidine mouse model for chronic alcoholic liver disease. *Lab Invest* **79:** 103–109.

Qiao J, Uzzo R, Obara-Ishihara T, Degenstein L, Fuchs E, Herzlinger D. 1999. FGF-7 modulates ureteric bud growth and nephron number in the developing kidney. *Development* **126:** 547–554.

Sato S, Sanjo H, Takeda K, Ninomiya-Tsuji J, Yamamoto M, Kawai T, Matsumoto K, Takeuchi O, Akira S. 2005. Essential function for the kinase TAK1 in innate and adaptive immune responses. *Nat Immunol* **6:** 1087–1095.

Shin S, Walton G, Aoki R, Brondell K, Schug J, Fox A, Smirnova O, Dorrell C, Erker L, Chu AS, et al. 2011. Foxl1-Cre-marked adult hepatic progenitors have clonogenic and bilineage differentiation potential. *Genes Dev* **25:** 1185–1192.

Srinivas S, Watanabe T, Lin CS, William CM, Tanabe Y, Jessell TM, Costantini F. 2001. Cre reporter strains produced by targeted insertion of EYFP and ECFP into the ROSA26 locus. *BMC Dev Biol* **1:** 4.

Steiling H, Werner S. 2003. Fibroblast growth factors: Key players in epithelial morphogenesis, repair and cytoprotection. *Curr Opin Biotechnol* **14:** 533–537.

Steiling H, Muhlbauer M, Bataille F, Scholmerich J, Werner S, Hellerbrand C. 2004. Activated hepatic stellate cells express keratinocyte growth factor in chronic liver disease. *Am J Pathol* **165:** 1233–1241.

Strick-Marchand H, Masse GX, Weiss MC, Di Santo JP. 2008. Lymphocytes support oval cell-dependent liver regeneration. *J Immunol* **181:** 2764–2771.

Suzuki A, Sekiya S, Onishi M, Oshima N, Kiyonari H, Nakauchi H, Taniguchi H. 2008. Flow cytometric isolation and clonal identification of self-renewing bipotent hepatic progenitor cells in adult mouse liver. *Hepatology* **48:** 1964–1978.

Tanimizu N, Miyajima A. 2007. Molecular mechanism of liver development and regeneration. *Int Rev Cytol* **259:** 1–48.

Tanimizu N, Nishikawa M, Saito H, Tsujimura T, Miyajima A. 2003. Isolation of hepatoblasts based on the expression of Dlk/Pref-1. *J Cell Sci* **116:** 1775–1786.

Terauchi A, Johnson-Venkatesh EM, Toth AB, Javed D, Sutton MA, Umemori H. 2010. Distinct FGFs promote differentiation of excitatory and inhibitory synapses. *Nature* **465:** 783–787.

Tichelaar JW, Lu W, Whitsett JA. 2000. Conditional expression of fibroblast growth factor-7 in the developing and mature lung. *J Biol Chem* **275:** 11858–11864.

Tirnitz-Parker JE, Viebahn CS, Jakubowski A, Klopcic BR, Olynyk JK, Yeoh GC, Knight B. 2010. Tumor necrosis factor-like weak inducer of apoptosis is a mitogen for liver progenitor cells. *Hepatology* **52:** 291–302.

Turanyi E, Dezso K, Csomor J, Schaff Z, Paku S, Nagy P. 2010. Immunohistochemical classification of ductular reactions in human liver. *Histopathology* **57:** 607–614.

Turner N, Grose R. 2010. Fibroblast growth factor signalling: From development to cancer. *Nat Rev Cancer* **10:** 116–129.

Yamamoto-Fukuda T, Aoki D, Hishikawa Y, Kobayashi T, Takahashi H, Koji T. 2003. Possible involvement of keratinocyte growth factor and its receptor in enhanced epithelial-cell proliferation and acquired recurrence of middle-ear cholesteatoma. *Lab Invest* **83:** 123–136.

Yanger K, Stanger BZ. 2011. Facultative stem cells in liver and pancreas: Fact and fancy. *Dev Dyn* **240:** 521–529.

Yovchev MI, Zhang J, Neufeld DS, Grozdanov PN, Dabeva MD. 2009. Thymus cell antigen-1-expressing cells in the oval cell compartment. *Hepatology* **50:** 601–611.

Zhang L, Rubins NE, Ahima RS, Greenbaum LE, Kaestner KH. 2005. Foxa2 integrates the transcriptional response of the hepatocyte to fasting. *Cell Metab* **2:** 141–148.

Zong Y, Panikkar A, Xu J, Antoniou A, Raynaud P, Lemaigre F, Stanger BZ. 2009. Notch signaling controls liver development by regulating biliary differentiation. *Development* **136:** 1727–1739.

Hepatology Research

Hepatology Research 2013 doi: 10.1111/hepr.12093

Original Article

Usefulness and accuracy of the international normalized ratio and activity percent of prothrombin time in patients with liver disease

Yasuhiro Takikawa, Mari Harada, Ting Wang and Kazuyuki Suzuki

Division of Gastroenterology and Hepatology, Department of Internal Medicine, Iwate Medical University, Morioka, Japan

Aim: In order to determine the most reliable reporting style for prothrombin time (PT) in patients with liver disease, we examined the correlations between the plasma antigen levels of clotting factors and the PT activity percent or two international normalized ratios (INR), and compared the inter-reagent variation among these PT reporting styles.

Methods: The PT was measured in 81 patients with liver diseases, including acute liver failure (ALF) ($n = 10$), acute liver injury ($n = 52$), chronic hepatitis ($n = 8$) and liver cirrhosis ($n = 11$), and in 75 warfarin-treated patients and 32 healthy volunteers. The PT of each plasma sample was determined with four commercial thromboplastins using an automated photo-optical coagulometer. For individual thromboplastin reagents, a locally determined international sensitivity index (local ISI) was derived using plasma obtained from healthy volunteers, warfarin-treated patients and liver disease patients. The INR_W and INR_{LD} were calculated using the corresponding local ISI. The PT activity percent was calibrated according to the Lineweaver–Burk equation. The PT values were compared with the plasma antigen levels of clotting factors X, II and VII measured using the enzyme-linked immunoassay method.

Results: The plasma factor X level was selected as the gold standard for measuring the synthetic liver function among the three clotting factors due to its significant relationship ($P = 0.007$) with the prognosis of ALF. The INR_{LD} exhibited the closest correlation to the factor X level ($r = 0.723$–0.759), with the smallest inter-reagent variation among these reporting styles.

Conclusion: The INR_{LD} is the most appropriate PT reporting style for use in patients with liver disease.

Key words: activity percent, international normalized ratio, liver failure, liver function test, prothrombin time

INTRODUCTION

THE PROTHROMBIN TIME (PT) is recognized to be a reliable marker of the protein synthetic function of the liver and thus a marker of the hepatic functional reserve. It is included in many authorized criteria for the diagnosis of liver failure and is used as an indication for liver transplantation worldwide.[1–8] The PT is directly measured as the clotting time (s) of citrated plasma mixed with a tissue thromboplastin reagent. Because the clotting time closely correlates with the concentrations of several clotting factors, including factors VII, X, V, II (prothrombin) and I (fibrinogen), it indicates the plasma levels of these clotting factors. These clotting factors are synthesized uniquely in hepatocytes and rapidly (several hours to a few days) disappear from the circulation after excretion from hepatocytes, in contrast to other liver-specific proteins such as albumin, which has a half-life of 2–3 weeks. In addition, the levels of clotting factors are hardly affected by the nutritional status of the patient, also in sharp contrast to albumin and prealbumin.[9] This is why the PT is considered to be an excellent and real-time marker of the protein synthetic function of the liver. However, the method used to report the results of PT measurement has not yet been standardized.

Although the international normalized ratio (INR) has been adopted in the model for end-stage liver disease (MELD) score and the diagnostic criteria of acute

Correspondence: Yasuhiro Takikawa, Division of Gastroenterology and Hepatology, Department of Internal Medicine, Iwate Medical University, 19-1 Uchimaru, Morioka 020-8505, Japan. Email: ytakikaw@iwate-med.ac.jp

Received 11 January 2013; revision 5 February 2013; accepted 6 February 2013.

liver failure in the USA,[6-8] its validity is controversial because it has been established as a marker for evaluating the effects of an oral anti-coagulant (warfarin), an antagonist of vitamin K carboxylase.[10] In contrast to the US criteria, the Japanese[8] and French (Clity) criteria[2,3] include the PT activity percent in the diagnostic criteria for acute liver failure (ALF). Indeed, one paper reported that activity percent is more accurate for evaluating liver damage than INR.[11] The important issues in comparing the validity of PT reporting methods are which method exhibits low variability across different laboratory conditions (thromboplastin reagents and equipment) and which method closely expresses the hepatic synthetic function.

In order to determine the superior reporting method for evaluating the hepatic functional reserve using PT, we analyzed the variability among different thromboplastin reagents (inter-reagent variation) and the correlations between the plasma antigen levels of clotting factors and INR and PT activity percent.

METHODS

Patients and plasma samples

THE PT WAS measured in 81 patients with liver diseases including ALF ($n = 10$), acute liver injury (hepatitis A, acute hepatitis B, drug-induced liver injury and unknown etiology) ($n = 52$), chronic hepatitis ($n = 8$) and liver cirrhosis (hepatitis B, hepatitis C and alcoholic hepatic injury) ($n = 11$), and in 75 warfarin-treated patients and 32 healthy volunteers.

Blood plasma samples were collected from 81 adult patients with liver disease, 75 adult patients who underwent stable warfarin treatment and 32 healthy adult volunteers using phlebotomy into vacutainer tubes containing 3.2% sodium citrate. Platelet-poor plasma was prepared using centrifugation at 2500 *g* for 15 min at 4°C, aliquoted and stored at −80°C until assay.

Thromboplastins and ISI calibration

Four thromboplastins that are commercially popular in Japan were selected for the present study, as listed in Table 1. The international sensitivity index (ISI) of each thromboplastin provided by the respective manufacturers was compared with the local ISI, which was calibrated according to the World Health Organization (WHO) guidelines for thromboplastins and plasma used to control oral anticoagulant therapy,[12] with the following differences: the use of frozen instead of fresh plasma, and the use of plasmas obtained from patients with liver disease and warfarin-treated patients instead of plasma obtained from patients on stable oral anticoagulation.

To reference standard thromboplastin in order to determine the ISI, the 3rd International Standard for human, recombinant plain thromboplastin (rTF/95, ISI 0.94) was obtained from a WHO laboratory (Central Laboratory of the Netherlands Red Cross blood transfusion service, Amsterdam, the Netherlands).

The PT (s) of the 32 healthy volunteers and the 75 warfarin-treated patients or 81 patients with liver disease were plotted on a double logarithmic scale with rTF/09 on the vertical axis and each commercial thromboplastin on the horizontal axis. The slope of the regression line was used as the ISI.

PT measurement and definition of ISI

The PT (s) of each plasma was determined with the four commercial thromboplastins using an automated photo-optical coagulometer, ACL TOP (Mitsubishi Chemical Medience, Tokyo, Japan) according to the manufacturer's instruction manual.

Table 1 Characteristics of thromboplastin reagents and determined ISI

Name	RecombiPlastin	Thrombocheck PT	Thromborel S	Coagpia PT-N
Manufacturer	Intrumentation Laboratory, Bedford, MA, USA	Sysmex, Kobe, Japan	Dade Behring, Deerfield, IL, USA	Sekisui Medical, Tokyo, Japan
Source	Human recombinant	Rabbit brain	Human placenta	Rabbit brain
ISI	1.01	1.70	1.01	1.07
Local ISI†	0.96	1.85	1.09	1.04
ISI_W	0.95	1.74	1.09	1.11
ISI_{LD}	0.95	1.30	0.94	0.96
Control PT (s)	10.5	11.8	12.5	12.8

†Local ISI values were calibrated for a photo-optical coagulometer, ACL TOP, using AK calibrant, which consists of four INR-known plasma samples.
INR, international normalized ratio; ISI, international sensitivity index; PT, prothrombin time.

For each individual thromboplastin, an ISI was calculated according to the WHO guidelines and defined as follows: ISI_W was defined as the locally determined ISI derived using plasma obtained from healthy volunteers and warfarin-treated patients, while ISI_{LD} was defined as the locally determined ISI derived using plasma obtained from healthy volunteers and patients with liver disease. Because the ISI provided by each manufacturer were calculated using an individually-fixed coagulometer but not always the ACL TOP, different ISI values might have been obtained when the thromboplastins were used in the ACL TOP. Therefore, we calculated the "local ISI" of each individual thromboplastin using the ACL TOP with AK calibrant (Technoclone, Vienna, Austria), which consists of four INR-known control plasmas (INR, 1.02, 2.13, 3.10 and 4.73). The local ISI of the individual thromboplastins were reverse calculated using simultaneous measurement of the PT of the AK calibrant with rTF/09 and each thromboplastin.

The INR was calculated using the formula: INR = (patient PT / control PT)^{ISI}, where the median value of the 32 healthy volunteer was used as the "control PT". The INR calculated using ISI_W or ISI_{LD} was represented as INR_W or INR_{LD}, respectively.

Calibration of PT activity percent

The PT (s) of each plasma with the four commercial thromboplastins was calibrated into the activity percent using a calibration equation (Lineweaver–Burk equation), obtained based on the regression between the reciprocal of a known activity percent of standard plasma (calibrant) and its measured PT (s) for three points made using stepwise dilution of the calibrant with the provided diluent.

The calibration equation for each thromboplastin was formulated using the calibrant provided by each representative manufacturer. In addition, two other activity percent values were calculated for each plasma using two other calibrants as common calibrants: calibrant A for RecombiPlastin and calibrant C for Thromborel S.

Enzyme-linked immunosorbent assay (ELISA) of the plasma clotting factors

The plasma antigen levels of factor II (prothrombin), factor VII and factor X were determined using ELISA with Assay Max Human Prothrombin, Assay Max Human Factor VII and Assay Max Human Factor X, respectively (AssayPro, St Charles, MO, USA), according to each manufacturer's instruction.

Statistical analysis

The central tendency of variants that showed a normal distribution was presented as the mean ± standard deviation (SD), while that of variants that showed another distribution type was presented as the median (25th–75th percentile).

The Mann–Whitney *U*-test was used to compare the mean values between two independent groups with respect to variants that did not show a normal distribution.

To compare correlation coefficients between the INR or activity percent and the antigen levels of clotting factors, each variant was first converted to a standard normal distribution with a mean of 0 and an SD of 1, then the Pearson product moment correlation coefficient was calculated.

The variability in PT among the four thromboplastin reagents (inter-reagent variation) was compared between different PT reporting styles using the Bland and Altman plot method, that is, the mean of the four PT values was determined according to the four different reagents in each plasma, and the differences between the maximum and minimum values among the four values were plotted on the horizontal axis and the vertical axis, respectively. The vertical axis was expressed according to two methods: raw differences in each PT reporting style and the ratio of the difference to the corresponding mean value.

RESULTS

Local ISI, originally determined ISI using plasma obtained from warfarin-treated patients (ISI_W) and liver disease patients (ISI_{LD})

THE ISI_W AND ISI_{LD} of the individual thromboplastins were compared with the local ISI and the manufacturer-provided ISI, as shown in Table 1. The ISI_W exhibited the closest approximation to the corresponding local ISI for each thromboplastin reagent, whereas the ISI_{LD} exhibited substantial differences from the local ISI. Because RecombiPlastin exhibited similar values among the ISI, it was thought to be a preferential thromboplastin provided by the WHO.

Association between the plasma antigen levels of clotting factors and the severity of acute liver injury

The plasma antigen levels of prothrombin, factor VII and factor X were compared between the acute liver injury

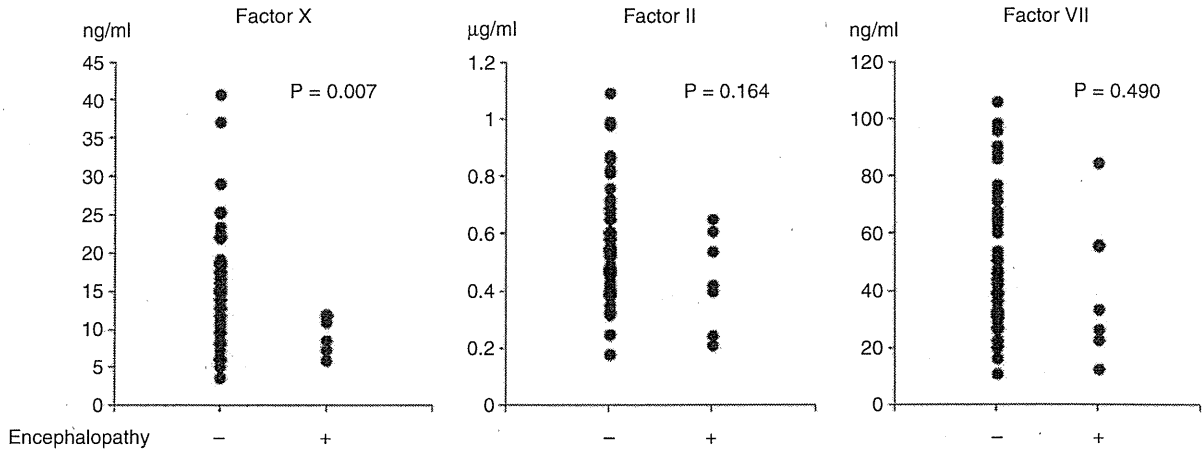

Figure 1 Differences in the plasma antigen levels of clotting factors X, II and VII between the patients with and without hepatic encephalopathy among those with acute liver injury. The *P*-values indicate the risk in Mann–Whitey *U*-test.

patients with and without hepatic encephalopathy (Fig. 1). Because only the factor X level significantly reflected the severity of liver damage among the three factors, we adopted the factor X level as the gold standard marker for the protein synthetic function of the liver.

Correlation between the INR or PT activity percent and the plasma antigen levels of clotting factors

Because the plasma antigen levels of factor X exhibited a logarithmic distribution (Fig. 2a), the values were converted to a normal distribution (mean = −2.609, SD = 0.446) (Fig. 2b) using the formula: x = LN (1 / factor X) and then standardized using the mean and SD. Similarly, the INR_W and INR_{LD} were converted to a normal distribution using the formula: x = LN (INR − 0.84), and then standardized using the individual mean and SD (Figs 3,4). Because the PT activity percent exhibited nearly normal or symmetrical distribution (data not shown), these values were directly standardized.

After the values were standardized, correlation coefficients between the plasma factor X levels and the INR_W, INR_{LD} and PT activity percent in the four different thromboplastins were calculated (Table 2). All five types of PT reporting styles were highly correlated with the plasma antigen levels of factor X. In particular, INR_{LD} exhibited largest correlation coefficient among the five types of PT reporting styles for every thromboplastin, while INR_W exhibited almost identical values to INR_{LD}. Therefore, the INR type reporting style of PT was always superior to the PT activity percent type reporting style for every thromboplastin reagent.

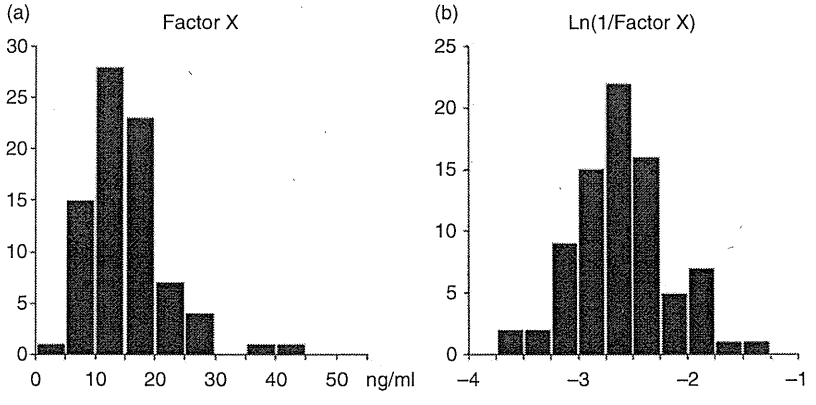

Figure 2 Distribution of the plasma antigen levels of factor X in the patients with liver disease. (a) Distribution of the crude values. (b) Distribution of the logarithmically converted values.

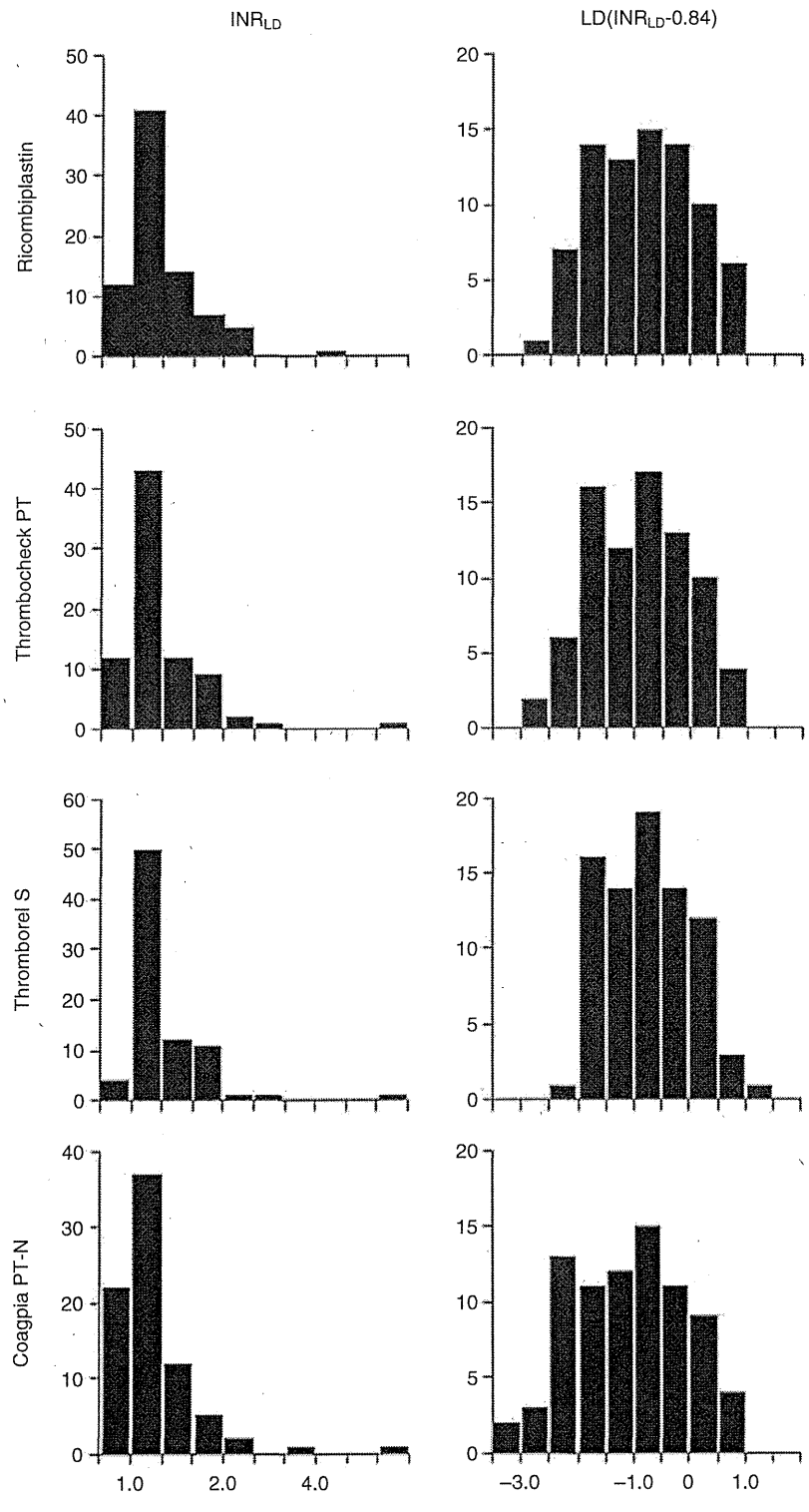

Figure 3 Distributions of the INR_{LD} values in patients with liver disease measured using four different reagents. The left side panel for each reagent indicates the distribution of the crude INR_{LD} values and the right side panel indicates the distribution of the logarithmically converted values.

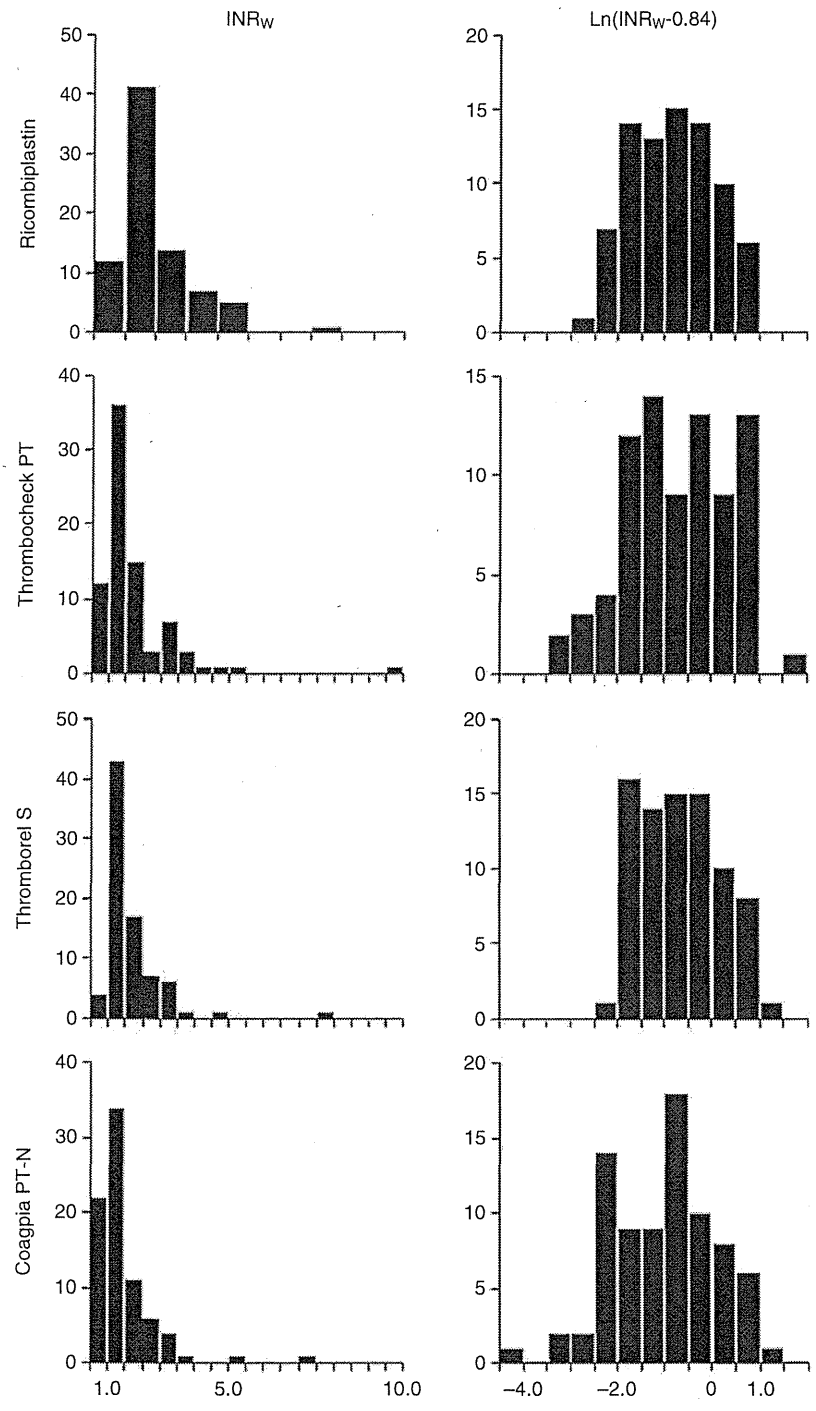

Figure 4 Distributions of the INR_W values in patients with liver disease measured using four different reagents. The left side panel for each reagent indicates the distribution of the crude INR_W values and the right side panel indicates the distribution of the logarithmically converted values.

For confirmation, we checked the correlation between each of these PT reporting styles and the level of prothrombin or factor VII. The factor VII level exhibited no significant correlation with any of the PT reporting styles. Although the prothrombin level showed a significant correlation with all three PT reporting styles, the correlation coefficients (0.44–0.54) were substantially lower than those of factor X.

Table 2 Comparison of correlation coefficients between the plasma factor X level and PT activity percent, INR_{LD} and INR_W in patients with liver disease

Reagents	PT activity percent			INR	
	Individual calibrant	Common calibrant for RecombiPlastin	Common calibrant for Thromborel S	INR_{LD}	INR_W
RecombiPlastin	0.717	0.717	0.720	0.734	0.734
Thrombocheck PT	0.678	0.666	0.696	0.744	0.726
Thromborel S	0.733	0.730	0.733	0.759	0.758
Coagpia PT-N	0.683	0.695	0.688	0.723	0.704

INR, international normalized ratio; PT, prothrombin time.

Inter-reagent variation of INR

The variability of the INR values among the thromboplastin reagents was compared between INR_W and INR_{LD} (Fig. 5). When the INR in the patients with liver disease was calculated using ISI_W (Fig. 5a), the differences among the thromboplastins were very large, especially in patients with a prolonged PT. In contrast, when the INR was calculated using ISI_{LD} (Fig. 5b), the differences among the thromboplastin reagents were substantially adjusted. As a result, the regression lines converged to the line, $y = x$, in INR_{LD}.

Inter-reagent variation of PT activity percent

Because the value of PT activity percent depends on both the sensitivity to the thromboplastin reagent and the accuracy of the calibrant titer, we used the same calibrant (a calibrant for RecombiPlastin) to examine the variability of PT activity percent depending on the difference in thromboplastin.

Although the variability among the thromboplastin reagents appeared to be smaller in lower PT activity percent samples (Fig. 6a), nearly 10% differences were seen in the area around the mean PT value of 20%. When the ratios of the maximum differences among the four reagents was plotted against mean PT values, the ratios were relatively high in both the normal PT and the highly prolonged PT areas (Fig. 6b).

Calibrant-dependent variation of PT activity percent

Because the inter-reagent variability of the raw PT activity percent was too high in the normal PT range (>80%)

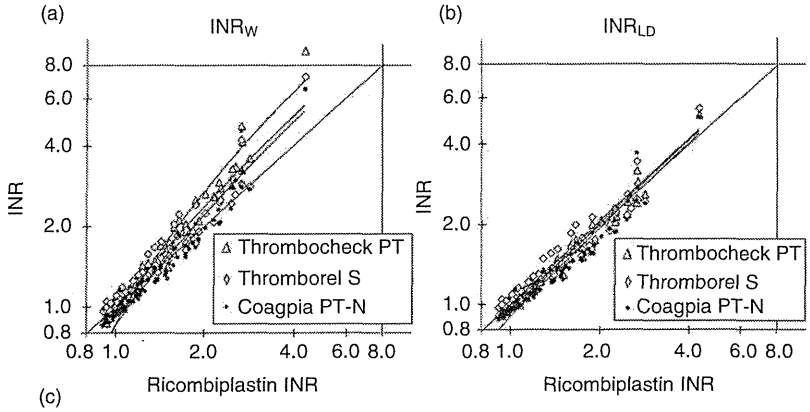

(c)

	INR_W		INR_{LD}	
	Regression line	r	Regression line	r
Thrombocheck PT	y=1.828x – 0.982	0.954	y=1.055x – 0.102	0.976
Thromborel S	y=1.388x – 0.423	0.944	y=1.056x – 0.055	0.956
Coagpia PT-N	y=1.349x – 0.503	0.947	y=1.042x – 0.146	0.957

Figure 5 Correlation between the international normalized ratio (INR) values in patients with liver disease measured with Thrombocheck PT, Thromborel S and Coagpia PT-N and those measured with RecombiPlastin. (a) Correlation between the INR_W and (b) INR_{LD} values. The lines in the graph indicate the regression lines. (c) Formulas of the regression lines. The *r*-values indicate the correlation coefficients. Δ, Thrombocheck PT; ◊, Thromborel S; ◆, Coagpia PT-N.

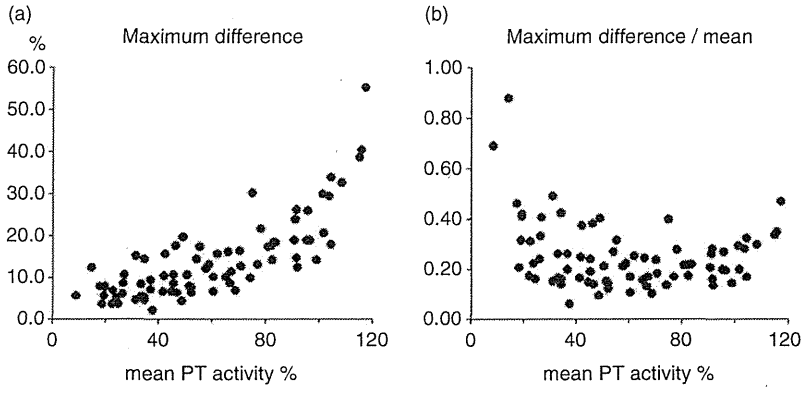

Figure 6 Inter-reagent variation in prothrombin time (PT) activity percent in the patients with liver disease. The horizontal line indicates the mean PT activity percent values measured using four different reagents in each samples. (a) The vertical lines indicate the maximum difference among the four values in each sample and (b) the ratio of the maximum difference to the mean value in each sample.

(Fig. 6) and the concerned range of the PT activity in clinical practice is below 80%, the inter-reagent variability and calibrant-dependent variability were examined regarding PT activity percent values lower than 80% (Table 3).

When the individually prepared calibrant was used, the maximum differences in the mean PT activity percent among the four thromboplastins was as high as 7.30%. The variability was relatively adjusted using common calibrants for RecombiPlastin and Thromborel S to 3.83 and 4.86, respectively.

On the other hand, the difference in the mean PT activity percent values among the reagents was very small (0.9) among the three thromboplastins except RecombiPlastin, even when the values were calculated using individually prepared calibrants.

DISCUSSION

ALTHOUGH THE PT is known to be a reliable marker of liver function, it is still controversial whether the activity percent and INR are appropriate for reporting the PT in patients with liver disease. In particular, in clinical practice for patients with ALF, the PT is indispensable for the diagnosis, prediction of prognosis and indications for liver transplantation. In Japan, ALF has been designated as an intractable disease on the national list, and the Japanese government has conducted many studies on ALF, including national surveys,[13–15] to establish and revise the diagnostic criteria[8,16] or the indications for liver transplantation,[17] and to develop potentially effective treatments for the disease. The diagnostic criteria have recently been revised to include the INR reporting style,[8,16] in addition to the activity percent used in the previous version of criteria, although the criteria did not advocate the adoption of any of these reporting styles as being appropriate in clinical practice for ALF patients.

To compare the usefulness of these different PT reporting styles, we examined whether the INR or PT activity percent is more closely associated with the hepatic synthetic function, and which values, INR_W, INR_{LD} or PT activity percent, demonstrate low inter-reagent variation.

Table 3 Comparison of the mean values of the PT activity percent in patients with liver disease among the four thromboplastin reagents in patients with liver disease

	Individual calibrant		Common calibrant for RecombiPlastin		Common calibrant for Thromborel S	
	Mean	SD	Mean	SD	Mean	SD
RecombiPlastin	48.1	18.2	48.1	18.1	45.8	17.1
Thrombocheck PT	40.8	17.9	45.5	20.6	42.4	17.6
Thromborel S	41.0	15.7	44.5	17.6	41.0	15.8
Coagpia PT-N	41.7	19.3	44.3	19.3	43.5	19.5
Maximum difference	7.30		3.83		4.86	

PT, prothrombin time; SD, standard deviation.